OPTIMAL TYRE MANAGEMENT FOR A FORMULA ONE CAR

by

Wilhelm Joachim West

Submitted in partial fulfillment of the requirements for the degree
Master of Engineering (Electronic Engineering)

in the

Department of Electrical, Electronic and Computer Engineering
Faculty of Engineering, Built Environment and Information Technology

UNIVERSITY OF PRETORIA

August 2020

SUMMARY

OPTIMAL TYRE MANAGEMENT FOR A FORMULA ONE CAR

by

Wilhelm Joachim West

Motorsport has become a multidisciplinary sport in which skilled engineers and strategists play as big a part in the team's success as the athlete driving the car. In Formula One it is common practice for teams to have dedicated resources on the track that are supported by a second team back at the home base who analyses telemetry data and performs simulations to refine the racing strategy. Optimal control calculations are typically used to optimise vehicle setup parameters (such as ride height and heave spring stiffness) and driver inputs (such as braking and steering) specific to each track.

Traditionally this approach has been employed by minimising time over a single lap. Although this is useful in qualifying simulations, there is an unexplored element of optimising a vehicle's "race pace". Drivers complete qualifying laps using minimal fuel with new tyres to get the best possible lap time but this performance cannot be sustained throughout the whole race. Drivers need to manage their tyres so that they do not wear prematurely and have a detrimental effect on their performance.

This work places an emphasis on tyre modelling and in particular how optimal control can be used to optimise a tyre management strategy. A model has been presented that reduces grip as a function of tyre wear. This ensures that the qualifying pace cannot be sustained indefinitely. A thermodynamic model consisting of two states (surface and carcass temperature) is used to calculate tyre wear, which ultimately dictates how much grip can be provided by each tyre.

The objective function for the optimal control problem is to minimise time over multiple laps and the absolute tyre wear (in mm tread) is constrained to a predefined limit. This ensures that the consequences of pushing the car to its limits are considered: overheating temperatures and accelerated wear will be detrimental to racing performance. The optimal control solver needs to manage the tyre temperatures carefully over a racing distance. It has been shown that lap times degrade more severely as the tyres reach the end of their life. At some point in the race this drop off in performance will render the car uncompetitive and strategists can use this model to evaluate the performance of different tyre compounds at each track and to strategically plan pit stops during a race.

ACKNOWLEDGEMENT

LIST OF ABBREVIATIONS

ABS	Anti-lock braking system
AD	Algorithmic differentiation
CFD	Computational fluid dynamics
COV	Calculus of variations
CSV	Comma-separated values
ERS	Energy recovery system
GPOPS	General purpose optimal control solver
IPOPT	Interior point optimizer
LSD	Limited slip differential
NLP	Non-linear programming
OCP	Optimal control problem
OCS	Optimal control solver
PMP	Pontryagin's minimum principle
SNOPT	Sparse nonlinear optimizer

TABLE OF CONTENTS

CHAPTER 1   INTRODUCTION

This chapter details the problem context and research gap addressed in this study. A summary is also given of the study objectives, as well as a hypothesis and research questions. The methods to evaluate the hypothesis and answer the research questions are listed. The research contribution highlights the novel approach and relevance of the work and lists the resulting publications. The chapter concludes with an overview of the study by highlighting the focus area of each chapter.

1.1   PROBLEM STATEMENT

1.1.1   Context of the problem

Optimal control techniques date back as far as 1697 when Johann Bernoulli published his solution to the brachistochrone problem [1]. The birth of optimal control theory however is believed to have its origin in the former Soviet Union with the work on Pontryagin's Maximum Principle [2] in the early 1960s. Today optimal control problems are found in a wide variety of subjects including engineering, economics and medicine [3].

Early efforts in the field of motorsport [4,5] used optimal control theory to determine how the idealized driver of a car or motorcycle would complete a certain manoeuvre in minimum time. A review of the historic applications of optimal control techniques to solve automotive problems can be found in Sharp and Peng [6]. The optimal control problem of having a Formula One car complete a lap around a race track in minimum time is of particular interest in this research, with emphasis being placed on tyre thermodynamics and wear.

1.1.2   Research gap

A mathematical model has been developed in [7, 8] which describe the dynamics of a race car moving around a track so that the optimal control problem can be solved. This model is under constant development, providing new insights each time that the model is expanded. In its simplest form the model consists of the following core components:

Track model

The race track is modelled as a flat surface in two dimensions using a curvilinear coordinate system. Distance travelled along the track centreline is used as the independent variable so that time can be minimized.

Vehicle dynamics

A rigid body approximation of the chassis is used. Longitudinal and lateral forces are produced by the tyres in reaction to the slip angle and normal loads. Vehicle dynamics are modelled by balancing the forces and moments that act on the chassis.

Aerodynamic loads

Aerodynamic loads consist of downforce and drag, which are dependent on velocity. The base model assumes that aerodynamic loads are applied at the vehicle's centre of pressure and that the coefficients for downforce and drag will remain constant.

Tyre model

The frictional forces of each tyre is modelled by an empirical relationship that is based on the Pacejka Magic Formula [9]. These frictional forces are responsive to the tyre's normal loads and combined slip.

Each core component identified above can be considered as an area of expertise that warrants further research. Various efforts have been made to build on the core model so that the behaviour of a Formula One car around a race track can be captured more closely. Figure 1.1 highlights the recent contributions to the model:

- In 2014 a significant change in the technical regulations of Formula One was implemented. All teams were required to recover thermal energy from the turbocharger to increase the green credentials of the sport. The modelling of a hybrid energy recovery system (ERS) [8] has shown that significant fuel savings are possible when ERS control is employed.

- A lot of the characteristics of a race track can only be described in three dimensions. Work has been done in 2015 to model the track as a ribbon in three dimensions [10, 11] instead of a flat surface in two dimensions. The track can now be described in terms of pitch, roll and heave, and accounts for elevation changes which will affect top speed and braking distances. Banked corners will alter grip through turns.

- The interactions between the suspension and aerodynamic performance were investigated in [12] and [13]. Kinematic analysis was used to develop a multi-link suspension model, which can be used to tailor suspension setup for each track.

- In 2016 a thermodynamic tyre model [14] was used to establish an optimal tyre warming and tyre usage strategy. Surface temperature is used to infer tyre grip and the sensitivity between tyre wear and lap time is explored. In this work the total tyre wear is calculated without establishing a relationship between wear and grip.
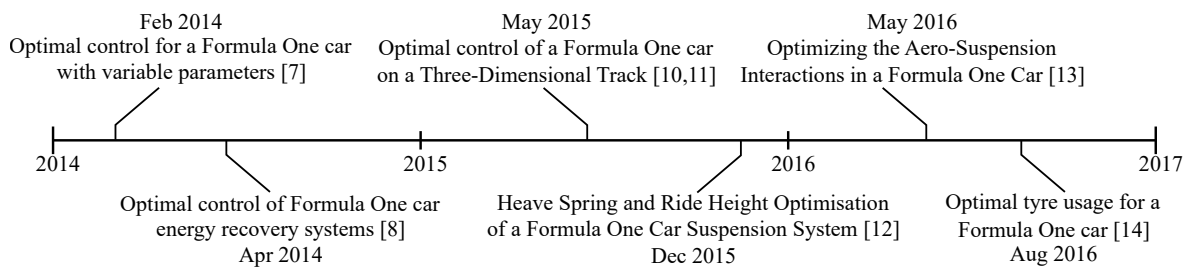
Figure 1.1. Chronological model developments.

Each contribution mentioned above [7, 8, 10–14] only considered the optimal control problem for a single lap. Even though tyre thermodynamics were included in [14] it only considered the tyre tread temperature and neglected temperature dynamics within the tyre carcass. The shortcoming of this one lap modelling approach is that it does not penalise performance due to tyres being worn. Even if the simulation would be repeated over multiple laps, the control input (and lap time) would be identical for each lap once the tyres are within the optimal temperature window rendering no useful information to develop a tyre management strategy.

The research gap identified is twofold: first and foremost the absence of a mechanism in the tyre model that will degrade racing performance as a result of wear and second is to solve the optimal control problem over multiple laps instead of only one.

1.2   RESEARCH OBJECTIVE AND QUESTIONS

The aim of this study is to build on the model given in [7, 8] by adding carcass temperature dynamics, introducing a mechanism that will penalise racing performance as a result of tyre wear and to utilise these additions to solve the optimal control problem over multiple laps. The resulting research questions for this study are:

- What is the impact of modelling the carcass temperature on the optimal control solution?
- Can a relationship between tyre wear and grip be established such that it accurately describes the degradation of performance over the course of a race?
- Which insights in developing a tyre management strategy can be gained from solving the optimal control of a Formula One car over multiple laps?

1.3   HYPOTHESIS AND APPROACH

The hypothesis is made that the thermodynamic influences of the tyre carcass will have a direct impact on the behaviour of the tread temperature and will therefore impact the solution to the optimal control problem. This effect will be exaggerated over multiple laps, making it increasingly difficult to manage tyre temperature throughout a race. Furthermore it is hypothesised that tyre wear will progressively degrade performance throughout a race and that the modelling thereof will guide racing teams to determine at which point during a race to consider a pit-stop and even help with the selection of tyre compounds for each track depending on their specific wear characteristics.

The following approach has been followed in this study:

1. The thermodynamic model presented in [14] has been expanded so that it can describe heat transfer effects between the tyre tread and carcass. The new model has been validated using telemetry data from a Formula One car.

2. A mechanism has been developed that will penalise racing performance as a result of tyre wear. This was achieved by modelling grip as a function of tyre wear.

3. The effect of adding a carcass temperature state and modelling grip as a function of tyre wear has been considered in isolation by means of computer simulation.

4. Finally the new model has been used to solve the optimal control problem over multiple laps. Conclusions are presented on how the model can be used to refine a tyre management strategy.

1.4 RESEARCH GOALS

The research goals can be summarised as follows:

- Add tyre carcass temperatures as an additional state to the existing model.
- Add tyre wear as an additional state to the existing model.
- Implement a mechanism that will penalise racing performance as a result of tyre wear.
- Solve the optimal control problem over multiple laps using the new model.
- Draw conclusions on how the model can be used to optimise a tyre management strategy.
- Develop a data visualisation tool that can be used to interpret the optimal control solution.

1.5 RESEARCH CONTRIBUTION

A novel method has been presented to model the degradation of racing performance as a result of tyre wear. Through the use of optimal control calculations it has been shown that the tyre carcass also contributes to suboptimal performance in a race if the tyres are not managed properly.

The following publications resulted from this work:

- W. J. West and D. J. N. Limebeer, "Optimal tyre management for a high-performance race car," *Vehicle System Dynamics*, pp. 1-19, August 2020.
- W. J. West and D. J. N. Limebeer, "Optimal Tyre Management of a Formula One car," *IFAC-PapersOnLine*, vol. xx, pp. xx, July 2020.

1.6 OVERVIEW OF STUDY

An overview of the structure of the dissertation is as follows:

- Chapter 2 contains a literature study on optimal control and tyre modelling. An overview is given on the commercial software that will be used to solve the optimal control problem.

- Chapter 3 derives the equations of the dynamic model that describes the motion of a Formula One car around a race track. This includes the thermodynamic model for the tyres with its associated wear mechanisms.

- Chapter 4 details how various simulations have been designed to validate the newly presented model which will ultimately be used to optimise a tyre management strategy.

- Chapter 5 provides a discussion on the results obtained from the simulations that were described in the previous chapter.

- Chapter 6 contains the dissertation conclusion.

- A user guide on how to use the data visualisation tool that has been developed is presented in Addendum A and the model parameters are given in Addendum B.

CHAPTER 2   LITERATURE STUDY

2.1   CHAPTER OVERVIEW

This chapter gives an overview of the optimal control techniques that will be used in this study followed by a discussion on tyre modelling.

2.2   OPTIMAL CONTROL BACKGROUND

The two most common methods used to simulate the trajectory of a race car around a track are the quasi-steady state and optimal control methods. Traditionally the quasi-steady state method was used because it is fast to compute and has proven to be very robust [15]. This method assumes that a lap can be divided into a series of steady state manoeuvres, which makes it unsuitable to study the vehicle's transient behaviour [12]. The formulation of an optimal control problem (OCP) is required to address this limitation.

2.2.1   Problem formulation

The purpose of optimal control is to determine the control inputs that will manipulate a system such that a certain performance criterion (also called the performance index) is maximised or minimised while the system is subject to physical constraints [16]. The system has a state vector $\boldsymbol{x}(t) \in \mathbb{R}^n$ and control vector $\boldsymbol{u}(t) \in \mathbb{R}^m$. In Bolza form the performance index is given by

$$J = \Phi(t_0, \boldsymbol{x}(t_0), t_f, \boldsymbol{x}(t_f)) + \int_{t_0}^{t_f} l(t, \boldsymbol{x}(t), \boldsymbol{u}(t)) \mathrm{d}t \qquad (2.1)$$

which is subject to the dynamic constraint

$$\dot{x}(t) = f(x(t), u(t), t), \tag{2.2}$$

the path constraint

$$c(x(t), u(t), t) \leq 0, \tag{2.3}$$

and the boundary condition

$$b(x(t_0), t_0, x(t_f), t_f) = 0. \tag{2.4}$$

The optimisation interval is given by $t_0 \leq t \leq t_f$ with t_f either fixed or a free optimisation parameter, depending on the type of problem being solved. The first term of the performance index Φ is the terminal cost function and depends only on the state variables at initial and final conditions. The second term of the performance index l is the state cost function and integrates the cost incurred during the entire trajectory.

2.2.2   Methods for solving the optimal control problem

Once a system has been described in the form of (2.1) to (2.4) a method must be chosen to obtain the optimal solution; refer to Figure 2.1 for a categorisation of widely adopted methods. A classical approach is to use calculus of variations (COV) to calculate the first order necessary conditions after which the Hamiltonian is minimised with respect to the control inputs, as stated by Pontryagin's Minimum Principe (PMP). This approach requires an analytical solution of the system equations and boundary conditions, which is seldom feasible for "real-world" problems [17].

In cases where an analytical solution is not feasible, the optimal control problem has to be transcribed into a non-linear programming problem (NLP) so that it can be solved numerically. This can be done in two ways: using a direct or an indirect method. In an indirect method the first-order optimality conditions are derived using the COV which results in a multiple-point boundary value problem [18]. A direct method discritises the state and/or controls which converts the optimal control problem into a parameter optimization problem [17]. In principle this means that an explicit derivation of the necessary conditions are not required for a direct method [19].

Regardless of the type of method that has been chosen, a solution can be obtained using either an explicit or implicit simulation technique. Explicit techniques integrate the system dynamics over

discrete intervals using approximations for the unknown boundary conditions. The approximations are iteratively adjusted until the error tolerances at the known boundary conditions are satisfied. Implicit techniques simultaneously solve the dynamics at each discritised time interval along with the boundary conditions without any notion of time-marching [20].
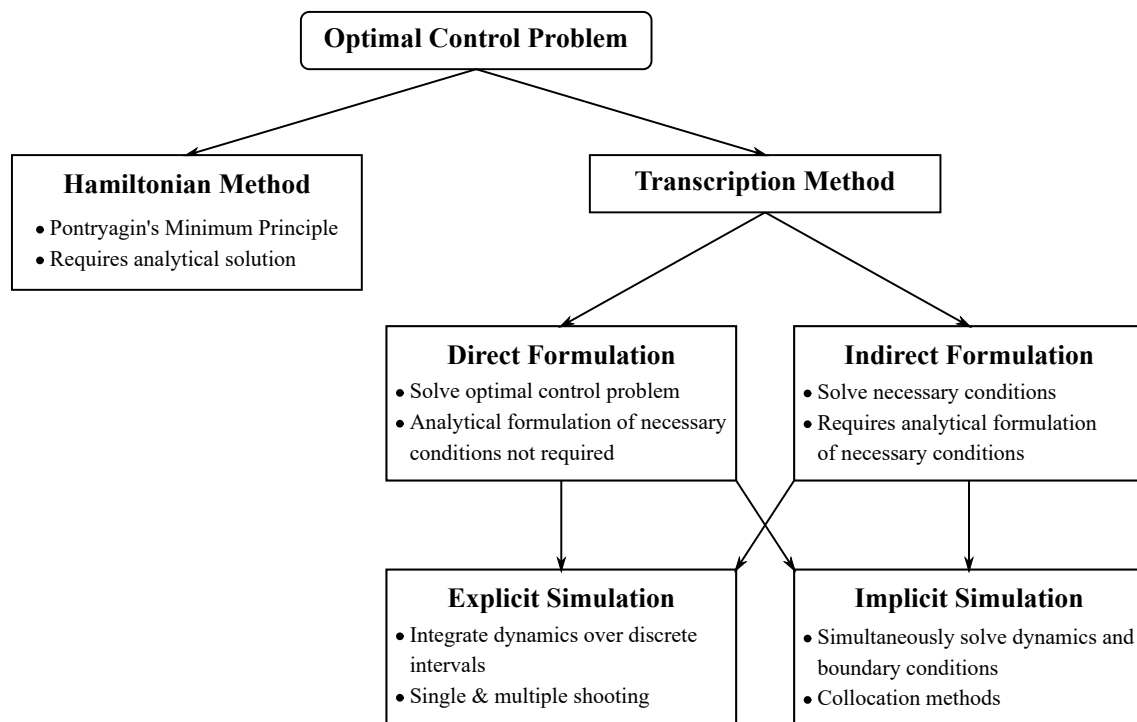
Figure 2.1. Categorisation of methods available to solve optimal control problems.

2.2.3   GPOPS-II

Present-day optimal control problems are most often solved numerically due to the complexity of the applications being considered [18]. The model for a Formula One car contains non-linear and non-smooth dynamics with both state and control constraints, which makes the choice in a numerical method appropriate. In the work presented here the general-purpose optimal control problem solver, GPOPS-II [3], is used to transcribe the infinite-dimensional OCP into a finite-dimensional optimisation problem with algebraic constraints. The software interfaces with the well known optimisation packages IPOPT [21] or SNOPT [22] to solve the resulting NLP, and employs hp-adaptive Gaussian quadrature collocation methods.

As was stated in the research goals (refer to Section 1.4), the tyre carcass temperature and tyre wear need to be added as additional states to the existing model. Seeing that a car has four wheels, it means that a total of eight new states will be added to the model. This significantly increases the amount of decision variables in the optimisation problem and emphasises the need to optimise the computing of the solution where possible. According to Rao in [18], several computational issues can be identified in the numerical solution of optimal control problems:

- Consistent approximations for the differential equation solutions.

- Proper scaling of the OCP.

- Exploitation of the sparsity in the NLP problem.

- Computation of derivatives.

Figure 2.2 shows the algorithmic flow used by GPOPS-II, and identifies three areas where optimisation can take place: scaling, choice of derivative supplier and choice of NLP solver.
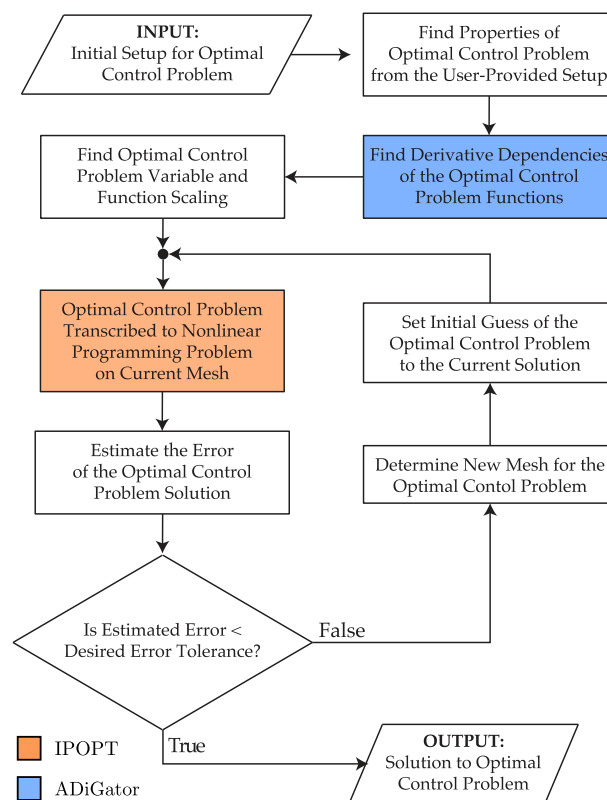
Figure 2.2. Flowchart for GPOPS-II algorithm (adapted from [3], with permission).

In the first place: care has been taken to properly scale the OCP that is provided as an input to the software seeing that convergence tolerances are necessarily based on the notion of "small" and "large" quantities [7]. Secondly, the open-source algorithmic differentiation tool, ADiGator [23], has been chosen as the derivatives supplier. Algorithmic differentiation (AD) uses the rules of differential calculus to numerically evaluate the derivatives of computer programs [24]. ADiGator has been designed to exploit the sparsity in each link in the chain rule which produces runtime efficient derivative files [23]. Lastly, to further leverage the benefits of using an AD provider, the choice has been made to use IPOPT as the NLP solver seeing that it can utilize second derivatives. This changes the solver from a quasi-Newton method (superlinear convergence near optimal solution) to a Newton method (quadratic convergence near optimal solution) [18]. Switching to ADiGator from the default derivate supplier (while keeping all other settings constant) resulted in a 30% reduction in computing time on an 8-core AMD Ryzen 3800X processor.

2.3 TYRE FUNDAMENTALS

2.3.1 Construction

Tyres are highly engineered structural composites that are designed to meet specific handling and performance criteria. They act as the sole interface between a vehicle and the road, enabling motion due to the frictional forces that are produced at the contact patch. It also acts as a spring and damper system to absorb road irregularities. The basic ingredients that are used to make tyres include polymers (consisting of natural or synthetic rubber), fillers to reinforce the rubber compounds, softeners such as petroleum oils to serve as processing aids, anti-degradents to protect tyres against degradation and curatives to promote vulcanisation [25]. Figure 2.3 illustrates the basic construction of a tyre.

A tyre consists of a rigid carcass which provides it with its basic shape and mechanical strength, and an outer tread layer that is typically constructed using a circumferential belt [26]. The sidewall, together with the gas that inflates the tyre, supports the belt and forms part of the vehicle suspension [27]. As a tyre rotates, its tread makes contact with and adheres to the road surface. The tread will deform as a result of frictional forces that prevent the tyre from slipping. When the deflection becomes too large to be maintained by the frictional forces, a portion of the tread in the contact patch will begin to slide [9]. The contact path is therefore divided into an adhesion and sliding region. Figure 2.4 shows an example

of the contact patch assuming it has a constant width c_w. In practice the contact patch is dependent on lateral and longitudinal forces, wheel camber and roughness of the road surface and will therefore not be rectangular in shape [27].
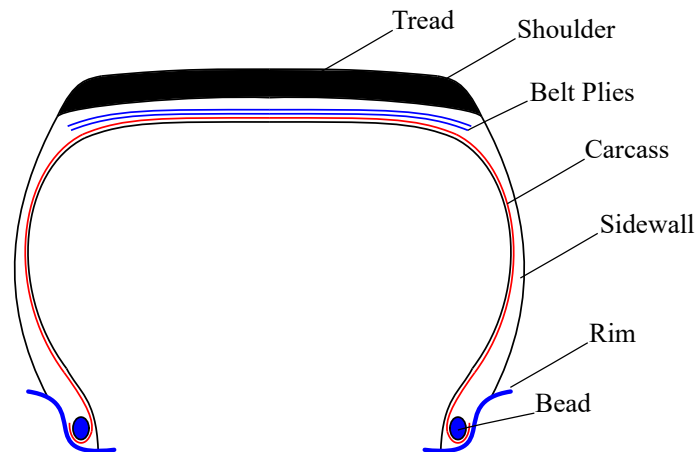
Figure 2.3. Tyre construction.
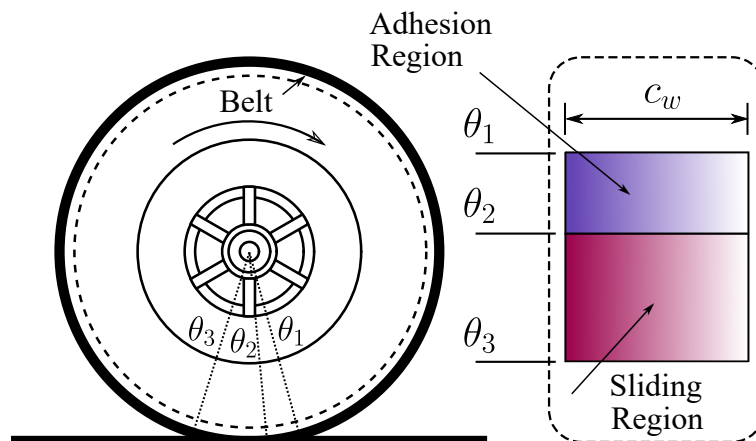
Figure 2.4. Illustration of tyre contact patch. It is assumed that a the

2.3.2 Tyre thermodynamics

The handling characteristics of a car are very sensitive to the operating temperature of the tyres [27]. Frictional and physical properties [28], such as braking and cornering stiffness, are directly influenced by the temperature profile of a tyre. Various approaches have been adopted to model tyre temperature, ranging from simpler lumped parameter models [14, 26, 27, 29] to complex finite element representations [28, 30–32].

Figure 2.5 visually illustrates the various approaches that were mentioned above. In illustration (1), a lumped parameter model has been used by Corollaro [29] which consists of a tread and carcass state. In illustration (2), Kelly & Sharp [26, 27] used a similar approach but added an additional state for the temperature of the gas inflating the tyre. The appeal in modelling the temperature of the inflation gas lies therein that it can be used to calculate the pressure of the gas, which in turn can be used to calculate the area of the contact patch. This requires a more complex tyre model to be used. It has been shown that minimal heat transfer occurs between the tyre carcass and inflation gas (see Figure 13 in [27]) and comparable thermodynamic results can be obtained by neglecting this state.

In illustration (3), Farroni [28, 30–32] used a finite element analysis to model temperature gradients across three states: the tyre tread, a bulk layer and the tyre inner liner. The bulk layer serves as an intermediate state between the tread and inner liner. The inner liner exchanges heat with the inflation gas, which is assumed constant (indicated by T_{inf} in Figure 2.5). This approach adds numerous extra states to the model, which renders large optimal control problems computationally intensive.

Kelly & Sharp were the only authors to model the pressure of the inflation gas. Even though this state may have a significant impact on tyre stiffness these effects were not considered, and the pressure was purely used to calculate the area of the contact patch.

In the work presented here, the lumped parameter model presented in [14] will be expanded by adding an additional thermodynamic state for the carcass temperature so that it takes on the form of illustration (1).
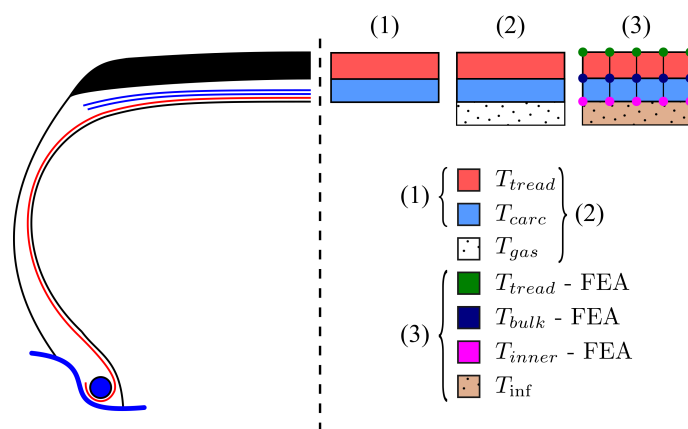
Figure 2.5. Comparison of various thermodynamic models.

2.3.3   Tyre wear

Tyre-focussed research has shown that the friction properties of tyre rubber are influenced by a number of factors including the tyre compound, track roughness, tyre loading, and the rubber temperature [33]. Of particular importance is the fact that tyre wear reduces the available friction, and consequently erodes the vehicle's long-stint race performance [34]. There is now substantial evidence to support a 'two-mechanism' theory of rubber abrasion [35]. The first predominates when the tread rubber experiences elastic surface deformations induced by frictional contact with road asperities. Under these conditions rubber particles are removed from the tread by a tensile tearing process. The second mechanism predominates when the rubber experiences a plastic contact with road asperities. This contact exists on a smaller scale and particles are removed by an abrasive-cutting action. The first mechanism is favoured by higher temperatures, low microtexture road surfaces, and soft tyre compounds. The second mechanism predominates at lower temperatures, on high microtexture road surfaces, and with harder tyre compounds.

The review article [36] discusses rubber abrasion, as well as the associated underlying theory and experiments. At moderate slip, wear increases as the square of the slip, and at constant slip, wear increases with increasing rubber stiffness, and decreases with increasing elastic hysteresis. Theoretical work presented in [37] is validated with a thin rigid wheel experiment. It is shown that at low slip the wear-rate is given by

$$\dot{w} = \frac{\gamma r f^2}{c};$$ (2.5)

where $\dot{w}$ is the volumetric of wear rate, γ represents the rubber's abradibility, r is the test wheel radius, f is the lateral force, and c is a measure of the wheel's stiffness. An example of a similar experimentally derived formula is available in the FTire model [38]. Care must be taken when considering the application of laboratory results based on solid wheels to real road tyres. The stiffness c in (2.5) refers to a rigid wheel, while in road tyre rigidity is dominated by the flexibility of the pneumatic chamber, the carcass, and the tread.

The influence of temperature is discussed in [36]. Their Figure 5 shows that the rubber abradibility increases at both low and high temperatures—this leads immediately to the idea that the tyre rubber's abradibility should be made a function of temperature. It also supports the 'two-mechanism' theory of rubber abrasion. As explained in [39], strong wear may occur at low temperatures where the rubber behaves as a glassy brittle material, and where the rubber can fracture by crack propagation.

At sliding velocities typical of a braking wheel, one expects large wear, with rubber particles being removed by brittle fracture. During sliding the road asperities exert oscillatory shear stresses on the tyre rubber, and at higher temperatures these shear stresses may break molecular bonds within the tread base material. This stress-assisted thermally-activated bond breaking gives rise to a rapid increase in high-temperature wear. The 'two-mechanism' theory of rubber abrasion leads us to expect a U-shaped wear characteristic of the form illustrated in Figure 2.6.
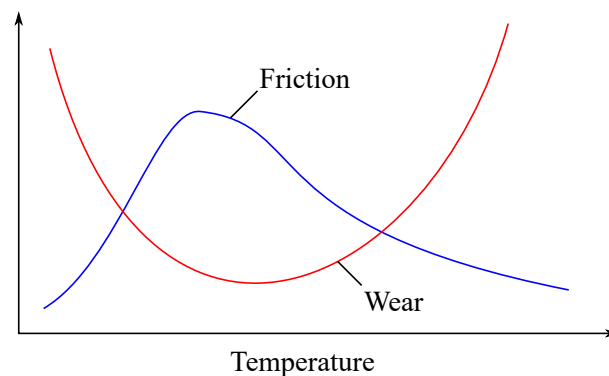
Figure 2.6. Temperature dependence of rubber friction and wear; based on experimental results in [40]. Adapted from [41], with permission.

The wear model used here follows [14], which is reminiscent of (2.5) in the optimum temperature operating range. It is important to note that wear is minimised at temperatures close to those associated with maximum friction.

2.3.4   Grip modelling

The forces produced at the contact patch of each tyre determine the motion (and therefore handling characteristics) of the car [26]. From a modelling perspective, grip is represented by the maximum friction that can be achieved by each tyre. Load transfer effects will reduce the normal forces acting on the lesser loaded tyres. The tyre with the lowest friction factor essentially becomes the limiting factor for acceleration. The frictional properties of racing tyres are especially sensitive to temperature, and maximum performance is only achievable in a relatively small temperature band [27]. Figure 2.7 illustrates that optimal grip (friction factor = 1) can only be obtained when the tread temperature lies between T_{p1} and T_{p2}. It becomes essential to manage tyres throughout a race to ensure that the available grip is maximised.
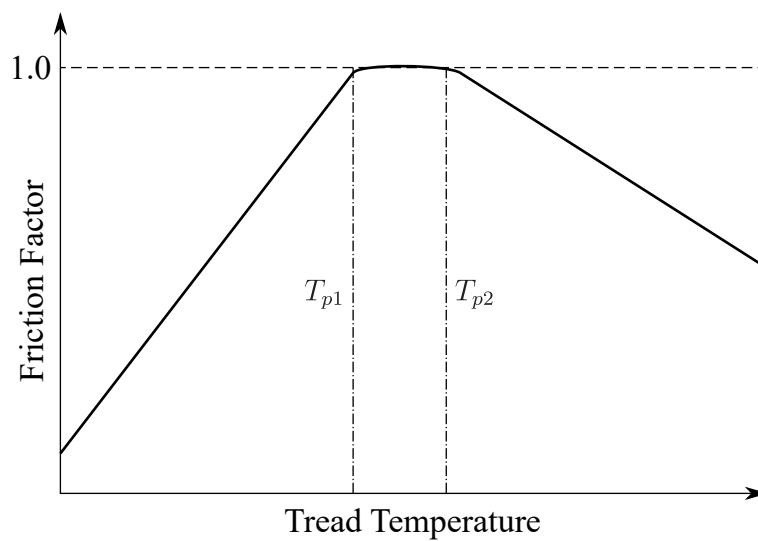
Figure 2.7. Optimal temperature window for racing tyre (taken from [42], with permission).

Tyre wear also plays an important role in handling performance. As a tyre is worn, the friction factor is permanently reduced which causes a decrease in driving forces at the ground [34]. The combination of the high cyclic stress and high temperatures that tyres are exposed to during a race results in mechanical and chemical changes in the rubber [43] which will accelerate the degradation process.

Figure 2.8 shows how different tyre types lose performance as the tyre degrades. Passenger tyres are typically designed for longevity, whereas racing tyres are designed to offer enhanced grip for a shorter time. The grip of the racing tyre initially increases and only starts to decrease after approximately 10 km of usage. This happens because racing tyres are not fully vulcanised during the manufacturing process [43]. During the initial wear phase the rubber goes through a curing process that form cross-links between sections of the rubber polymer chains. This curing process increases the grip, rigidity and durability of the tyre [44].
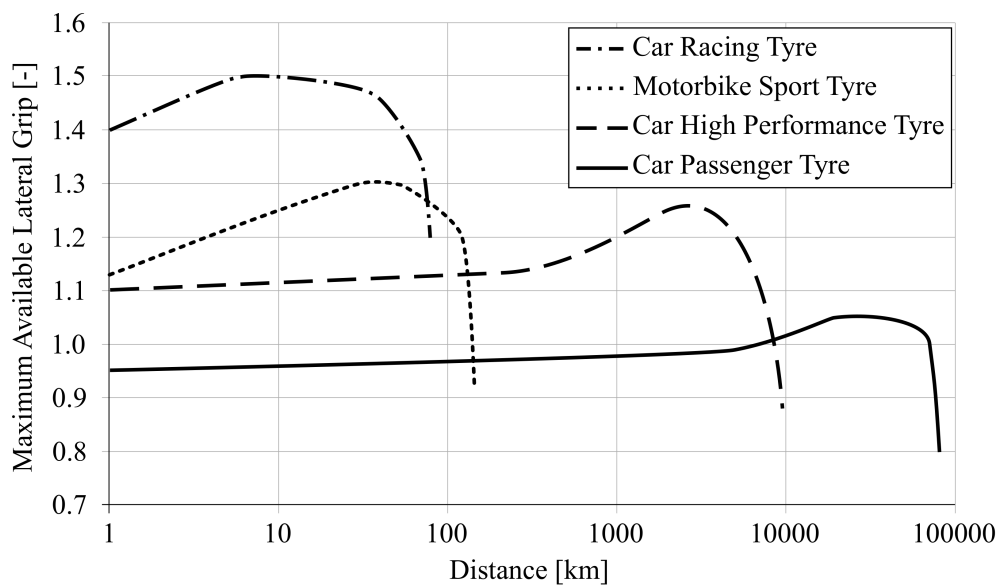
Figure 2.8. Handling performance decrease due to wear for different tyres (adapted from [34], with permission).

2.4   CONCLUSION

In the literature review various aspects of tyre modelling were discussed. Grip ultimately translates to racing performance and the modelling thereof plays a critical role in solving the optimal control problem. Various approaches in modelling temperature dynamics have been considered. A simpler two-state model that retains the fundamental thermodynamic characteristics is favoured above models of higher computational complexity. Tyre temperature has been shown to influence grip levels, with peak friction only being attainable in a narrow temperature band. Grip can also be modelled as a function of tyre wear. Seeing that suboptimal temperature management can lead to accelerated tyre wear, this work will combine the temperature and wear effects on tyre grip as a novel contribution to this research so that racing performance can be evaluated over multiple laps.

CHAPTER 3   MODEL DESCRIPTION

3.1   CHAPTER OVERVIEW

This chapter discusses the various components of the model that will be used to solve the optimal control problem. The system being described in this work is that of a Formula One car driving around a race track. It can be described by a series of differential and algebraic equations, which will be derived in the following sections. The model has to be described in terms of a certain independent variable. In this particular case two choices are available: time t and distance travelled along the track centreline s, of which the latter will be used. The advantage of using distance travelled as independent variable instead of time is that an explicit connection with the track position can be maintained. This section is based on the model that has been developed in previous work and can be found in [7] and [8].

3.2   TRACK MODEL

The track is mapped out on a curvilinear coordinate system where the track centreline forms the abscissa (indicated by the dash-dotted line in Figure 3.1). Distance travelled along the centreline s is the independent variable where the origin is denoted by the start-finish line of the track. Any point along the track is described by the track radius $\mathcal{R}$ at that point. The vehicle's position perpendicular to the track centreline is described by the vector $\mathfrak{n}$ where $\mathfrak{t}$ is the centreline's tangent vector. These vectors are based on a fixed inertial reference frame and have components (n_x, n_y) and (t_x, t_y) respectively. For the vehicle to remain within the track boundaries, the magnitude of $\mathfrak{n}$ may not exceed the length of half the track's width $\mathcal{N}$ which yields the path constraint

$$|\mathfrak{n}| \leq \mathcal{N}. \tag{3.1}$$
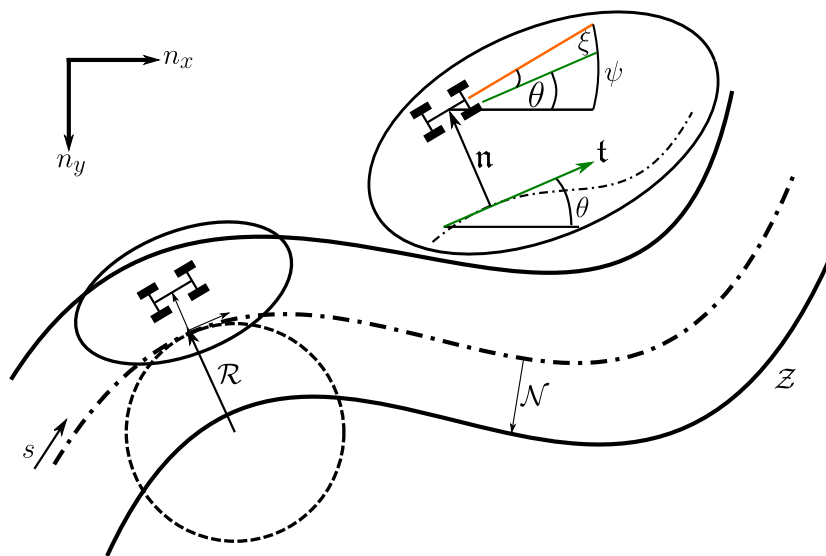
Figure 3.1. Curvilinear-coordinate description of track segment $\mathcal{Z}$ (adapted from [7], with permission).

Direction may be described relative to the track or inertial reference frame. The angle between the vehicle and track tangent vector is given by ξ, whereas the angle between the vehicle and inertial reference frame is given by ψ (which is called the absolute yaw). These two parameters are related to each other by the track orientation angle θ and be calculated by

$$\psi = \theta + \xi. \tag{3.2}$$

The curvilinear axis is related to the Cartesian reference frame by using the track orientation angle. Figure 3.2 (a) shows an incremental change along the track centreline, ds. As this approaches an infinitesimally small change, ds can be approximated by a straight line which forms a right triangle with the inertial reference frame. It follows from elementary trigonometry that

$$\mathrm{d}x = \mathrm{d}s\cos\theta \tag{3.3}$$

$$\mathrm{d}y = \mathrm{d}s\sin\theta \tag{3.4}$$

$$\Rightarrow \frac{\mathrm{d}y}{\mathrm{d}x} = \tan\theta \tag{3.5}$$

$$\Rightarrow \theta = \arctan\frac{\mathrm{d}y}{\mathrm{d}x}. \tag{3.6}$$

Track curvature $\mathcal{C}$ is defined as the inverse of the radius. Figure 3.2 (b) shows an incremental change in track orientation, dθ. As this approaches an infinitesimally small change, the arc length ds can be calculated by assuming that the radius $\mathcal{R}$ remains constant.

(a) Incremental arc length ds on track segment $\mathcal{Z}$.

(b) Geometric relationship between θ and s.
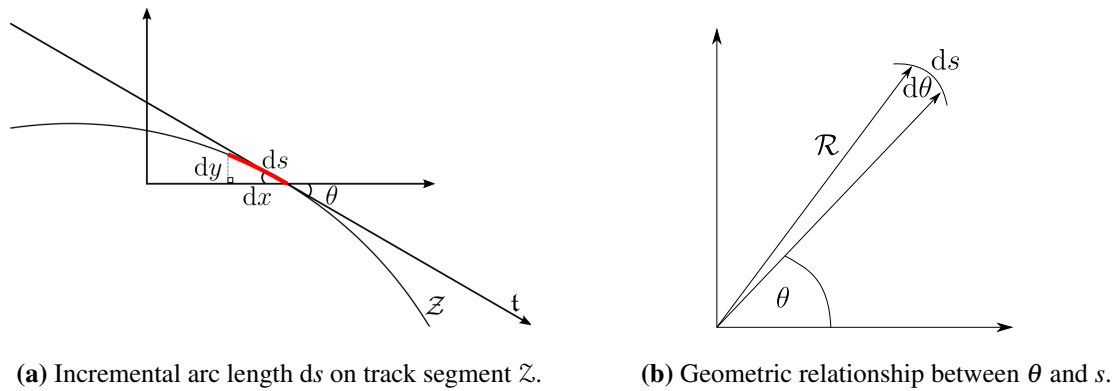
Figure 3.2. Track geometry derived from elementary trigonometry.

It follows from elementary trigonometry that

$$\mathrm{d}s = \mathcal{R}\mathrm{d}\theta \tag{3.7}$$

$$\Rightarrow \frac{1}{\mathcal{R}} = \frac{\mathrm{d}\theta}{\mathrm{d}s} = \mathcal{C}. \tag{3.8}$$

By definition the vehicle has longitudinal velocity u in the direction of travel and lateral velocity v that is orthogonal to the longitudinal component (refer to Figure 3.3 for a diagram of the special case where there is no offset between the vehicle and track centreline). These velocities can be resolved in the direction of $\hat{\mathfrak{n}}$ and $\hat{\mathfrak{t}}$ which are the directional vectors of $\mathfrak{n}$ and $\mathfrak{t}$ respectively:

$$u_{\hat{\mathfrak{t}}} = u\cos\xi \tag{3.9}$$

$$u_{\hat{\mathfrak{n}}} = u\sin\xi \tag{3.10}$$

$$v_{\hat{\mathfrak{t}}} = -v\sin\xi \tag{3.11}$$

$$v_{\hat{\mathfrak{n}}} = v\cos\xi. \tag{3.12}$$
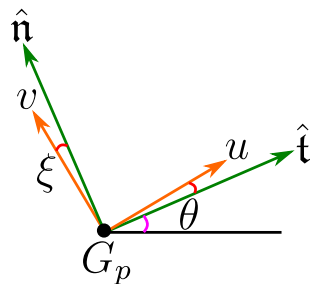
Figure 3.3. Velocity vector diagram for vehicle travelling at point G_p that lies on the track centreline.

It is important to note that (3.9) to (3.12) is expressed in terms of the **vehicle's own reference frame**. The change in track curvature will result in an angular velocity component that needs to be accounted for when the velocity is expressed in terms of the **track centreline's reference frame**. It follows that the vehicle velocity, in terms of the track centreline reference frame, is given by:

$$\dot{s} = u\cos\xi - v\sin\xi + n\dot{\theta} \tag{3.13}$$

$$\dot{n} = u\sin\xi + v\cos\xi. \tag{3.14}$$

Equation (3.13) can be rearranged as follows:

$$\dot{s} - n\dot{\theta} = u\cos\xi - v\sin\xi \tag{3.15}$$

$$\Rightarrow \dot{s}\left(1 - \frac{n\dot{\theta}}{\dot{s}}\right) = u\cos\xi - v\sin\xi \tag{3.16}$$

$$\Rightarrow \dot{s}\left(1 - n\frac{d\theta}{dt}\frac{dt}{ds}\right) = \dot{s}\left(1 - n\frac{d\theta}{ds}\right) = u\cos\xi - v\sin\xi. \tag{3.17}$$

Substituting (3.8) into (3.17) yields

$$\dot{s}\left(1 - n\mathcal{C}\right) = u\cos\xi - v\sin\xi \tag{3.18}$$

$$\Rightarrow \dot{s} = \frac{u\cos\xi - v\sin\xi}{1 - n\mathcal{C}}. \tag{3.19}$$

Differentiating (3.2) with respect to time yields

$$\dot{\xi} = \dot{\psi} - \dot{\theta}. \tag{3.20}$$

Substituting (3.8) into (3.20) yields

$$\dot{\xi} = \dot{\psi} - \frac{d\theta}{ds}\frac{ds}{dt} = \dot{\psi} - \mathcal{C}\dot{s}. \tag{3.21}$$

The rate at which yaw angle changes, $\dot{\psi}$, is redefined as ω for use in the following section:

$$\dot{\psi} \equiv \omega. \tag{3.22}$$

The track related differential equations are given in (3.14), (3.19) and (3.21). These equations represent derivates with respect to time, and need to be transformed to represent derivates with respect to s. This is done using the factor S_f, which is defined as the inverse of $\dot{s}$:

$$S_f(s) = \frac{dt}{ds} = \frac{1 - n\mathcal{C}}{u\cos\xi - v\sin\xi}. \tag{3.23}$$

The resulting differential equations are obtained by multiplying (3.14) and (3.21) with S_f on both sides of the equal sign:

$$\frac{dn}{ds} = S_f(u\sin\xi + v\cos\xi) \tag{3.24}$$

$$\frac{d\xi}{ds} = S_f(\dot{\psi} - \mathcal{C}). \tag{3.25}$$

3.3 VEHICLE MODEL

A standard rigid-body representation of a chassis with longitudinal, lateral and yaw freedoms will be used in this work. Four-wheel braking and a limited-slip differential is assumed to control the wheel torque distribution.

3.3.1 Dynamic model

For modelling purposes the vehicle's position is reduced to a single point acting at the centre of mass. Figure 3.4 shows the yaw angle ψ, lateral velocity v and longitudinal velocity u at this point. The steering angle δ is defined as the angle between the direction in which the front wheels are facing and the direction in which the vehicle is travelling (longitudinally). The relevant geometric quantities required for the force and moment balances are defined in Figure 3.5.
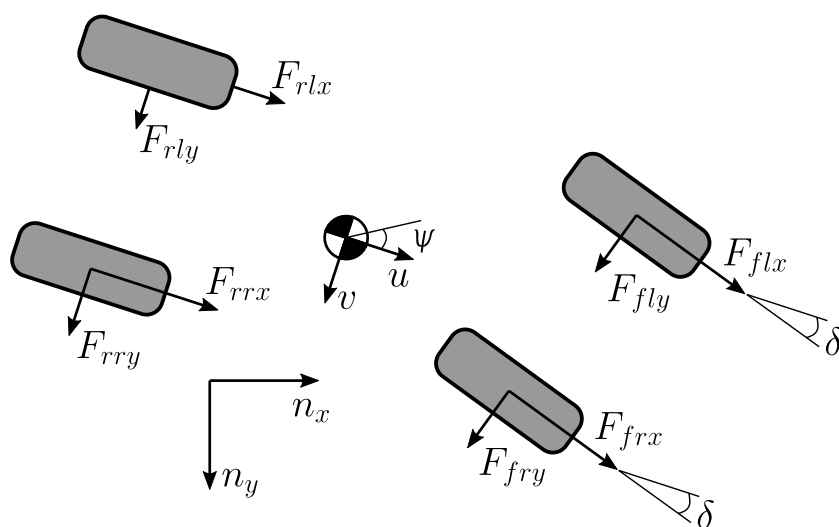
Figure 3.4. Tyre force system (adapted from [7], with permission).
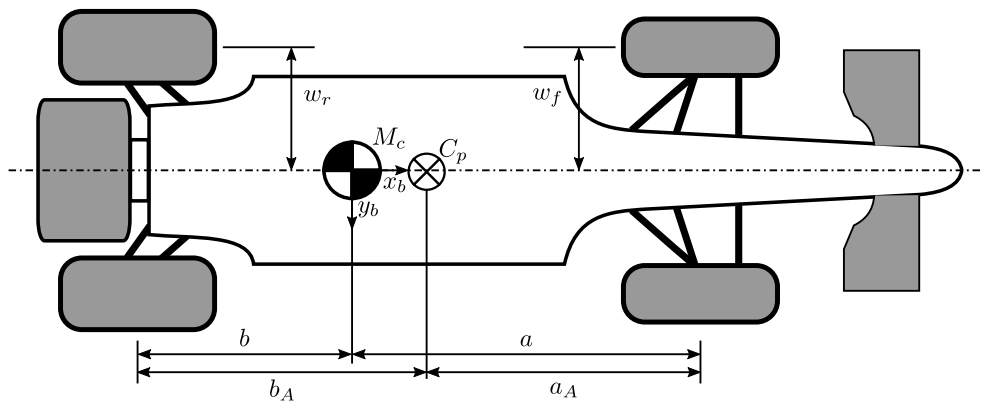
Figure 3.5. Vehicle geometric parameters (adapted from [8], with permission).

The forces that act on the vehicle are experienced at the contact patch between each tyre and the road surface (which is indicated as "C" in Figure 3.6). Tyre forces are produced in reaction to the weight of the vehicle pushing down on the road and also to the tyres' slip when the car is in motion. Tyre slip can be calculated using the empirical formulae given in Section 3.4.1.
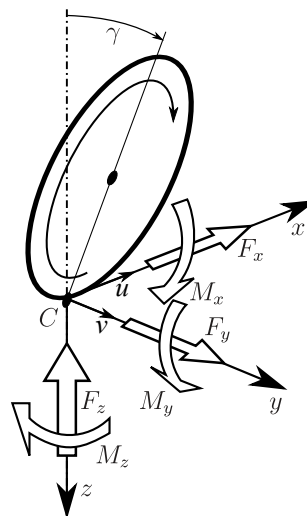
Figure 3.6. Tyre forces and moments (taken from [42], with permission).

Tyre forces have three components [42]: longitudinal force F_x, cornering (side) force F_y and normal force (load) F_z. Each one of these forces has a corresponding moment: the overturning couple moment M_x, rolling resistance moment M_y and the yawing moment M_z. Vehicle dynamics are described by balancing the forces and moments that act on the vehicle. The two-dimensional track model used in this research assumes that the road is a flat surface and will therefore not account for wheel camber, which is equivalent to $\gamma = 0$ in Figure 3.6.

The longitudinal and lateral force balances together with the yaw moment balance are given in (3.26) to (3.28) respectively:

$$M\frac{\mathrm{d}}{\mathrm{dt}}u(\mathrm{t}) = M\omega v + F_x \tag{3.26}$$

$$M\frac{\mathrm{d}}{\mathrm{dt}}v(\mathrm{t}) = -M\omega u + F_y \tag{3.27}$$

$$I_z\frac{\mathrm{d}}{\mathrm{dt}}\omega(\mathrm{t}) = a\Big(\cos\delta(F_{fry} + F_{fly}) + \sin\delta(F_{frx} + F_{flx})\Big) + w_f(\sin\delta F_{fry} - \cos\delta F_{frx})$$

$$- w_r F_{rrx} + w_f(\cos\delta F_{flx} - \sin\delta F_{fly}) + w_r F_{rlx} - b(F_{rry} + F_{rly}), \tag{3.28}$$

where M is the vehicle mass, I_z is the moment of inertia about the z-axis and the quantities a, a_A, b, w_f and w_r are shown in Figure 3.5.

Longitudinal and lateral forces F_x and F_y are calculated as follows:

$$F_x = \cos\delta(F_{frx} + F_{flx}) - \sin\delta(F_{fry} + F_{fly}) + (F_{rrx} + F_{rlx}) + F_{ax} \tag{3.29}$$

$$F_y = \cos\delta(F_{fry} + F_{fly}) + \sin\delta(F_{frx} + F_{flx}) + (F_{rry} + F_{rly}), \tag{3.30}$$

where F_{ax} is the aerodynamic drag force.

Unless the tyres are limited by friction, the powertrain will deliver the maximum engine power $P_{\max}$. The maximum torque provided to the rear axle is constrained by:

$$u(F_{rrx} + F_{rlx}) \leq P_{\max}. \tag{3.31}$$

Time dependent equations can once again be expressed in terms of the independent variable s:

$$\frac{\mathrm{d}u}{\mathrm{d}s} = S_f(s)\dot{u} \tag{3.32}$$

$$\frac{\mathrm{d}v}{\mathrm{d}s} = S_f(s)\dot{v} \tag{3.33}$$

$$\frac{\mathrm{d}\omega}{\mathrm{d}s} = S_f(s)\dot{\omega}. \tag{3.34}$$

3.3.2 Load transfer effects

Load transfer refers to the change in load borne by each wheel. As a vehicle enters a corner, inertial forces will effectively "pull" the car towards the outer edge of the track. This shifts the weight of the vehicle from the inside tyres (closest to the apex of the corner) to the outside tyres. The same effect is observed under braking and acceleration; in this case the load shifts between the front and rear axle.

Seeing that the vehicle is assumed to have no elastic suspension components, the rolling and pitching moments will be directly influenced by changes in wheel load distribution. Moment balances around the vehicle's body-fixed x_b and y_b axes (refer to Figure 3.5) are given in (3.35) and (3.36) respectively, which is followed by a vertical force balance in (3.37):

$$0 = w_r(F_{rlz} - F_{rrz}) + w_f(F_{flz} - F_{frz}) + hF_y \tag{3.35}$$

$$0 = b(F_{rrz} + F_{rlz}) - a(F_{frz} + F_{flz}) + hF_x + (a_A - a)F_{az} \tag{3.36}$$

$$0 = F_{rrz} + F_{rlz} + F_{frz} + F_{flz} + Mg + F_{az}, \tag{3.37}$$

where the quantities a, b, w_f, w_r and h are shown in Figure 3.5.

There is one less linear equation than what there are unknown variables in the load transfer equations (we have four tyre forces with three equations; F_{az} is calculated using (3.40)). In order to obtain a unique solution a suspension-related roll balance will be added where the lateral load difference across the front axle is expressed as some fraction of the whole:

$$F_{frz} - F_{flz} = D_{roll}(F_{frz} + F_{rrz} - F_{flz} - F_{rlz}), \tag{3.38}$$

where D_{roll} is the parameter that is used to describe the fraction.

3.3.3 Aerodynamic loads

Formula One cars make use of multi-link suspension systems which play a crucial role in the aerodynamic performance of the vehicle. The kinematics of a race car can be modelled as a function of the suspension's motion, of which some examples include the ride height h_r and suspension induced roll ϕ_r which are shown in Figure 3.7. Down force and drag coefficients can be mapped as a function of these suspension interactions to provide a more accurate reflection of the vehicle's aerodynamic performance. These coefficients are typically derived from track and wind tunnel measurements [42].

A simplified approach will be taken for the purposes of this research where aerodynamic loads are computed as a function of the vehicle's velocity and suspension interactions are neglected. It is assumed that aerodynamic forces are applied at vehicle's the centre of pressure. The drag and down forces are given by (3.39) and (3.40) respectively:

$$F_{ax} = -\frac{1}{2}C_D(u)\rho A u^2 \tag{3.39}$$

$$F_{az} = -\frac{1}{2}C_L(u)\rho A u^2, \tag{3.40}$$

where C_D is the drag coefficient, C_L is the down force coefficient, ρ is the air density and A is the vehicle's frontal area.
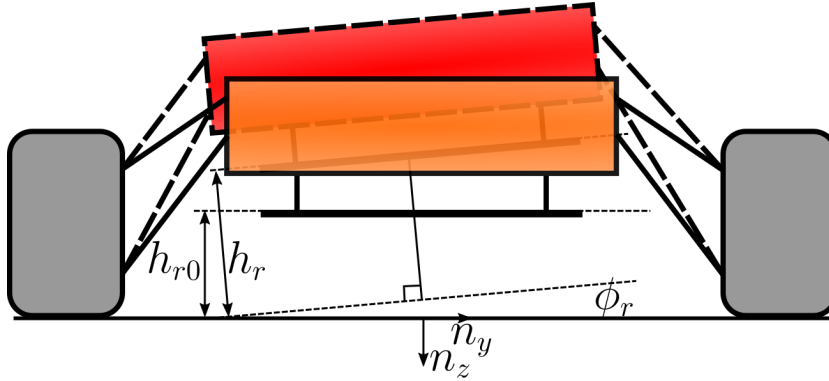
Figure 3.7. Suspension travel of vehicle moving into a right-hand bend (adapted from [13], with permission).

3.3.4 Wheel torque distribution

It is assumed that equal pressure is applied to the brake calipers on each axle ($F_{frx} = F_{flx}$). When a wheel "locks up" however the braking torque applied to the rotating wheel will be more than the torque applied to the locked wheel (and therefore $F_{frx} \neq F_{flx}$). In modern passenger cars an anti-lock braking system (ABS) will prevent this from happening but most racing regulations forbid the use of such driving aids. Locking of the front wheels will be modelled using the following constraint:

$$0 = \max(\omega_{fr}, 0)\max(\omega_{fl}, 0)(F_{frx} - F_{flx}), \tag{3.41}$$

where ω_{fr} and ω_{fl} are the angular velocities of the front right and front left wheels respectively. When a wheel locks up it will result in a negative angular velocity in which case the braking torque constraint will be inactive.

A limited slip differential (LSD) will allow the wheels on the rear axle to rotate at different speeds. To allow this in the model, the following constraint is introduced:

$$R(F_{lrx} - F_{rrx}) = k_d(\omega_{rl} - \omega_{rr}), \tag{3.42}$$

where ω_{rl} and ω_{rr} are the angular velocities of the rear left and rear right wheels, R is the wheel radius and k_d is a torsional damping coefficient.

The max function has an undefined derivate at $x = 0$, and can be approximated using:

$$\max(\omega, 0) = \frac{\omega + \sqrt{\omega^2 + \varepsilon^2}}{2}, \tag{3.43}$$

where ε is a 'small' constant (see [42] p416).

3.4   TYRE MODEL

Tyres forces are described by a combined-slip magic formula that accounts for longitudinal and lateral load transfer effects. A lumped parameter model will be used to account for tyre thermodynamics. Wear is modelled as a function of temperature and frictional power.

3.4.1   Tyre Friction

The frictional forces of each tyre is modelled by an empirical relationship that is based on the Pacejka Magic Formula [9]. These frictional forces are responsive to the tyre's normal loads and combined slip. The tyre's longitudinal slip κ and lateral slip α is given by:

$$\kappa = -\left(1 + \frac{R\omega_w}{u_w}\right) \tag{3.44}$$

$$\tan \alpha = -\frac{v_w}{u_w}, \tag{3.45}$$

where R is the wheel radius, ω_w the angular velocity of the wheel, u_w the longitudinal and v_w the lateral component of the wheel's velocity measured at the centre of the wheel relative to its body-fixed axis.

The peak values and locations of the longitudinal and lateral friction coefficients are determined using linear interpolation [26]:

$$\mu_{x\max} = (F_z - F_{z1})\frac{\mu_{x\max 2} - \mu_{x\max 1}}{F_{z2} - F_{z1}} + \mu_{x\max 1} \tag{3.46}$$

$$\mu_{y\max} = (F_z - F_{z1})\frac{\mu_{y\max 2} - \mu_{y\max 1}}{F_{z2} - F_{z1}} + \mu_{y\max 1} \tag{3.47}$$

$$\kappa_{\max} = (F_z - F_{z1})\frac{\kappa_{\max 2} - \kappa_{\max 1}}{F_{z2} - F_{z1}} + \kappa_{\max 1} \tag{3.48}$$

$$\alpha_{\max} = (F_z - F_{z1})\frac{\alpha_{\max 2} - \alpha_{\max 1}}{F_{z2} - F_{z1}} + \alpha_{\max 1}, \tag{3.49}$$

where subscripts '1' and '2' refer to measured tyre parameters.

Tyre slip is normalised with respect to the peak slip:

$$\kappa_n = \frac{\kappa}{\kappa_{\max}} \qquad (3.50)$$

$$\alpha_n = \frac{\alpha}{\alpha_{\max}}. \qquad (3.51)$$

The normalised slip coefficients are used to calculate a combined slip coefficient:

$$\rho = \sqrt{\alpha_n^2 + \kappa_n^2}. \qquad (3.52)$$

This in turn is used to calculate the longitudinal and lateral friction coefficients:

$$\mu_x = \mu_{x\max} \sin\left(Q_x \arctan(S_x \rho)\right) \qquad (3.53)$$

$$\mu_y = \mu_{y\max} \sin\left(Q_y \arctan(S_y \rho)\right), \qquad (3.54)$$

where Q_x and Q_y are the longitudinal and lateral shape factors.

The parameters S_x and S_y are given by:

$$S_x = \frac{\pi}{2 \arctan(Q_x)} \qquad (3.55)$$

$$S_y = \frac{\pi}{2 \arctan(Q_y)}. \qquad (3.56)$$

The longitudinal and lateral components of the tyre forces are calculated using:

$$F_x = \mu_x F_z \frac{\kappa_n}{\rho} \qquad (3.57)$$

$$F_y = \mu_y F_z \frac{\alpha_n}{\rho}. \qquad (3.58)$$

Lateral slip α at each wheel is given by:

$$\alpha_{rr} = \arctan\left(\frac{v - \dot\psi b}{u - \dot\psi w_r}\right) \qquad (3.59)$$

$$\alpha_{rl} = \arctan\left(\frac{v - \dot\psi b}{u + \dot\psi w_r}\right) \qquad (3.60)$$

$$\alpha_{fr} = \arctan\left(\frac{\sin\delta(\dot\psi w_f - u) + \cos\delta(\dot\psi a + v)}{\cos\delta(u - \dot\psi w_f) + \sin\delta(\dot\psi a + v)}\right) \qquad (3.61)$$

$$\alpha_{fl} = \arctan\left(\frac{\cos\delta(\dot\psi a + v) - \sin\delta(\dot\psi w_f + u)}{\cos\delta(\dot\psi w_f + u) + \sin\delta(\dot\psi a + v)}\right). \qquad (3.62)$$

Longitudinal slip κ at each wheel is given by:

$$\kappa_{rr} = -\left(1 + \frac{R\omega_{rr}}{u - \dot{\psi}w_r}\right) \tag{3.63}$$

$$\kappa_{rl} = -\left(1 + \frac{R\omega_{rl}}{u + \dot{\psi}w_r}\right) \tag{3.64}$$

$$\kappa_{fr} = -\left(1 + \frac{R\omega_{fr}}{\cos\delta(u - \dot{\psi}w_f) + \sin\delta(\dot{\psi}a + v)}\right) \tag{3.65}$$

$$\kappa_{fl} = -\left(1 + \frac{R\omega_{fl}}{\cos\delta(u + \dot{\psi}w_f) + \sin\delta(\dot{\psi}a + v)}\right). \tag{3.66}$$

Tyre friction influences are commonly depicted on tyre curves. Figure 3.8 shows how longitudinal tyre force varies with longitudinal slip under various loads and side slip conditions (similar curves can be generated for lateral force versus lateral slip). The special case of pure longitudinal slip ($\alpha = 0°$) is considered on the left-hand side. It is shown that larger longitudinal forces are available when the normal load is increased. The right-hand side shows how longitudinal force is adversely affected by lateral slip. The peak of the curve is flattened as slip increases, which reduces the ability of the tyre to provide grip.
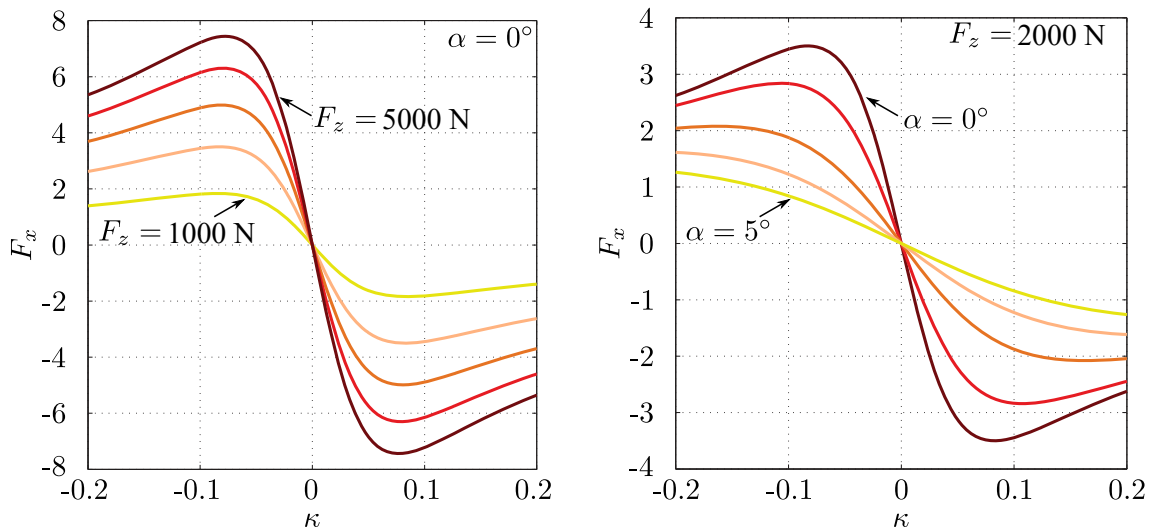
Figure 3.8. Longitudinal tyre force versus longitudinal slip. Five normal loads are considered at zero lateral slip on the left-hand diagram. Normal loads increase in intervals of 1000 N. Five lateral slip angles are considered at a fixed normal load of 2000 N on the right-hand diagram. Side slip angles increase in intervals of 1° (adapted from [14], with permission).

3.4.2   Thermodynamic model

The car tyre thermodynamics are modelled using tyre-carcass and tyre-surface temperature states—this is an extension of the model proposed in [14]. The number of free model parameters has been reduced from six to three. The track temperature, and the ambient temperature of the surrounding air, are treated as constant. The tyre-surface temperature state is associated with the tread. The tyre's carcass temperature state is used to represent the temperature of the tyre's bulk material including the metal core and side-wall rubber. The high thermal conductivity of the metal core lends support to the isotropic modelling assumption.

Figure 3.9 represents the lumped parameter model used to describe the thermodynamic behaviour of the tyres:
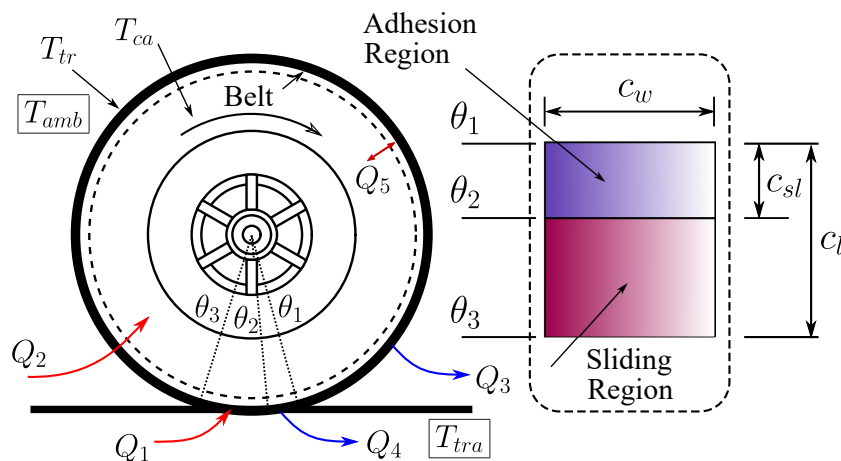
Figure 3.9. Thermodynamic model with dominant heat flows

The tyre model comprises four temperatures and five heat flows as detailed in Table 3.1. We will assume that:

1. Q_1 is generated due to slippage in the tyre's sliding region [42],

2. Q_2 is generated by virtue of structural flexing of the carcass,

3. Q_3 is heat lost by convective cooling,

4. Q_4 represents heat lost by conductive cooling in the adhesion region of the contact patch, and

5. Q_5 is the is heat transfer between the tread and the carcass.

Table 3.1. Tyre temperatures and heat flows

Item	Description
T_{amb}	Ambient temperature (asssumed fixed)
T_{tra}	Track temperature (asssumed fixed)
T_{tr}	Tread temperature
T_{ca}	Carcass temperature
Q_1	heat generated in the tyre sliding region
Q_2	heat generated due to tyre carcass deflection
Q_3	heat loss due to convective cooling
Q_4	conductive cooling in the adhesion region of the contact patch
Q_5	heat flow between the tread and the carcass

A lumped parameter model was used in [14] to represent the thermal behaviour of racing tyres during a single-lap simulation. In that study the tyres were modelled as single isotropic masses that are subject to multiple heat flows. This model is now expanded by adding a carcass temperature state, with its associated heat transfer equations. The differential equations for the tyre tread temperature, T_{tr}, and the tyre carcass temperature, T_{ca}, are obtained by simple energy balances:

$$m_t c_t \frac{\mathrm{d}}{\mathrm{d}t} T_{tr} \;=\; Q_1 - Q_3 - Q_4 + Q_5 \tag{3.67}$$

$$m_c c_c \frac{\mathrm{d}}{\mathrm{d}t} T_{ca} \;=\; Q_2 - Q_5; \tag{3.68}$$

where m_t and m_c are the tread and carcass masses, and c_t and c_c are respectively the tread and carcass specific heat capacities.

The heat generated in the sliding region of the contact patch is calculated by summing the longitudinal and lateral slip powers

$$Q_1 = p_1 u_n (|F_x \kappa| + |F_y \tan \alpha|), \tag{3.69}$$

where the tunable parameter p_1 represents the portion of frictional power that goes to heating the tread. The slip quantities α and κ, and the tyre forces F_x and F_y are calculated using formulae given in Section 3.4.1.

The longitudinal velocity u_n at each wheel is given by:
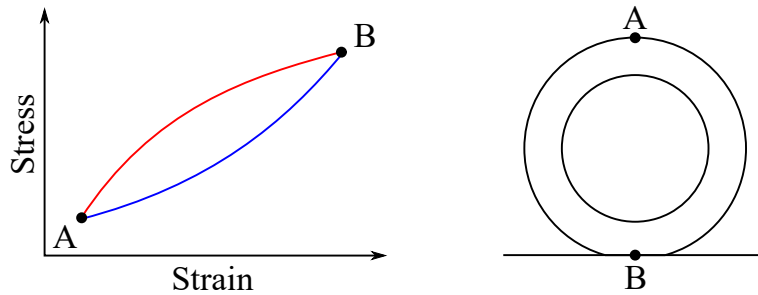
$$u_{n,rr} = u - \dot{\psi}w_r \tag{3.70}$$

$$u_{n,rl} = u + \dot{\psi}w_r \tag{3.71}$$

$$u_{n,fr} = \cos\delta(u - \dot{\psi}w_f) + \sin\delta(\dot{\psi}a + v) \tag{3.72}$$

$$u_{n,fl} = \cos\delta(\dot{\psi}w_f + u) + \sin\delta(\dot{\psi}a + v). \tag{3.73}$$

As the wheels rotate, the carcass undergoes cyclic loading and relaxation, which causes the carcass to warm [45]. This type of information can be obtained by direct measurement; see Figure 2 in [30]. Figure 3.10 shows the stress-strain cycle along with the extreme points *A* and *B*.

Figure 3.10. Hysteresis heating and extreme points of stress-strain cycle.

For a given material, the work done per cycle per unit volume, ΔE, corresponds to the area under the hysteresis curve; ΔE is a non-linear function of the temperature and the inflation-induced initial stress. If the rolling diameter is D, the heating power is of the form $Q_2 = \frac{u_n m_c}{\pi D}\Delta E$. Since the heating process is anisotropic, the tyre carcass deflection heating is represented by

$$Q_2 = p_2 \frac{u_n m_c}{\pi D}\left(k_1|F_x| + k_2|F_y| + k_3|F_z|\right), \tag{3.74}$$

where p_2 is a tunable parameter, and k_1, k_2 and k_3 are used to recognise the anisotropic character of the tyre's construction. The constants k_1, k_2 and k_3 are given in Table B.1, while p_2 is fitted to measured track data.

The heat loss due to convection between the tyre tread and the surrounding ambient air is given by:

$$Q_3 = h_{forc}A_{conv}(T_{tr} - T_{amb}) \tag{3.75}$$

where

$$A_{conv} = A_{tot} - c_w c_l, \tag{3.76}$$

is the area accessible to the ambient air flow.

The first term on the right-hand side of (3.76) is the total surface area of the tread

$$A_{tot} = \pi D W, \tag{3.77}$$

while the second term is the area of the tread in contact with the road.

The tread contact patch width of the front and rear tyres are given by c_{wf} and c_{wr} respectively; see Table B.1. The lengths of the contact patches c_l are calculated using [14]:

$$c_l = a_{cp} F_z^{0.7}. \tag{3.78}$$

The heat transfer coefficient h_{forc} is determined using an empirical formula that correlates well with Computational Fluid Dynamics (CFD) simulation [30]:

$$h_{forc} = \frac{K_{air}}{L}\left[0.0239\left(\frac{uL}{v_{air}}\right)^{0.805}\right]. \tag{3.79}$$

The conductivity and kinematic viscosity of air, are K_{air} and v_{air} respectively, and are evaluated at the average temperature between the tread and ambient air. Numerical values can be found in material physical property databases—see for example Table A–9 [46]; u is the forward velocity of the vehicle.

The characteristic length of the heat exchange surface is given by:

$$L = \frac{1}{1/D + 1/W}, \tag{3.80}$$

where D is the tyre diameter and W the tread width.

The conductive heat loss from the tyre tread to the track is given by Newton's cooling law:

$$Q_4 = h_{tt} A_{cp}(T_{tr} - T_{tra}), \tag{3.81}$$

where h_{tt} is the transfer coefficient of conduction between the track and the tread [27].

The non-sliding area of the contact patch A_{cp} is the given by:

$$A_{cp} = c_w c_s(\alpha) c_l. \tag{3.82}$$

The function $c_s(\alpha)$ gives the proportion of the contact patch length in the non-sliding region of the tread as the vehicle approaches its cornering limit (see Figure 3.9):

$$c_s(\alpha) = \frac{\alpha}{\alpha_c}(c_{s2} - c_{s1}) + c_{s1}, \tag{3.83}$$

where c_{s1} and c_{s2} are reference values given in Table B.1, while α_c is the reference slip angle.

The heat transfer between the tread and carcass is given by:

$$Q_5 = p_3 A_{tot}(T_{carc} - T_{tread}), \tag{3.84}$$

where p_3 is a tunable heat transfer coefficient of conduction, and A_{tot} is given in (3.77).

3.4.3 Parameter fitting

The free model parameters were estimated using a least squares fitting between measured telemetry data and the calculated temperature states from the model. It is assumed that the tyres were at operating temperatures when the data were collected. No telemetry data were available for the carcass temperatures, which vary relatively slowly. The tread and carcass temperatures were constrained to be cyclic in the parameter optimisation process to ensure that the obtained solution remains physically realisable despite the fact that carcass telemetry data were absent. Literature containing measured inner temperature data can be found in Figure 8 of [30]. The best-fit parameter set for each tyre is shown in Figure 3.11 with an average root mean square error of 6.0 °C between the four tyres. The slow carcass temperature behaviour is attributable to its greater thermal inertia as compared to the thin tread layer. In essence, the carcass acts as a heat store that prevents the tread from cooling down to the track temperature. Table B.5 shows the parameters that resulted in the best fit for each tyre.

Figure 3.12 shows the heat flows through each tyre. The rear-left tread and carcass temperatures begin the high-speed lap at approximately at 100 °C, which is well below the optimal operating temperature; see Figure 3.14. The tread then cools on the high-speed straight of approximately 750 m before the car enters turn 1. On this initial section the tyre experiences very little sliding friction Q_1, modest deflection heating Q_2, significant, but decreasing convective cooling Q_3, almost no conductive cooling Q_4, and an increasing level of heat transfer to the rapidly cooling tread Q_5.

The car then slows on the entry to turn 1, and the tread begins to heat up under firm braking due to increased Q_1. There is a decrease in the deflection heating Q_2 due to reduced wheel speed, the

convective heating Q_3 reduces, the conductive cooling Q_4 remains small, and the heat transfer between the tread and carcass Q_5 reduces. The car then accelerates into the high-speed turn 3. Under firm acceleration and high lateral force loads, the rear-left tyre experiences over 30 kW of friction heating Q_1, the deflection heating Q_2 increases, as the speed increase, and the convection cooling Q_3 increases too–(3.79) is a function of speed. The conductive cooling Q_4 remains small, while Q_5 sees an increase.

Towards the end of turn 3 the tread temperature increases to approximately 150 °C. The tyre then cools on the straight leading to turn 4. Further heating occurs on the entry to turn 4, with the tyre then cooling again on the straight between turns 4 and 5. Another temperature peak of approximately 140 °C occurs under braking in turn 9. The tread temperature behaviour for the remainder of the lap can be explained in much the same way. As expected, the tread temperature varies rapidly, while the carcass temperature varies much more slowly.
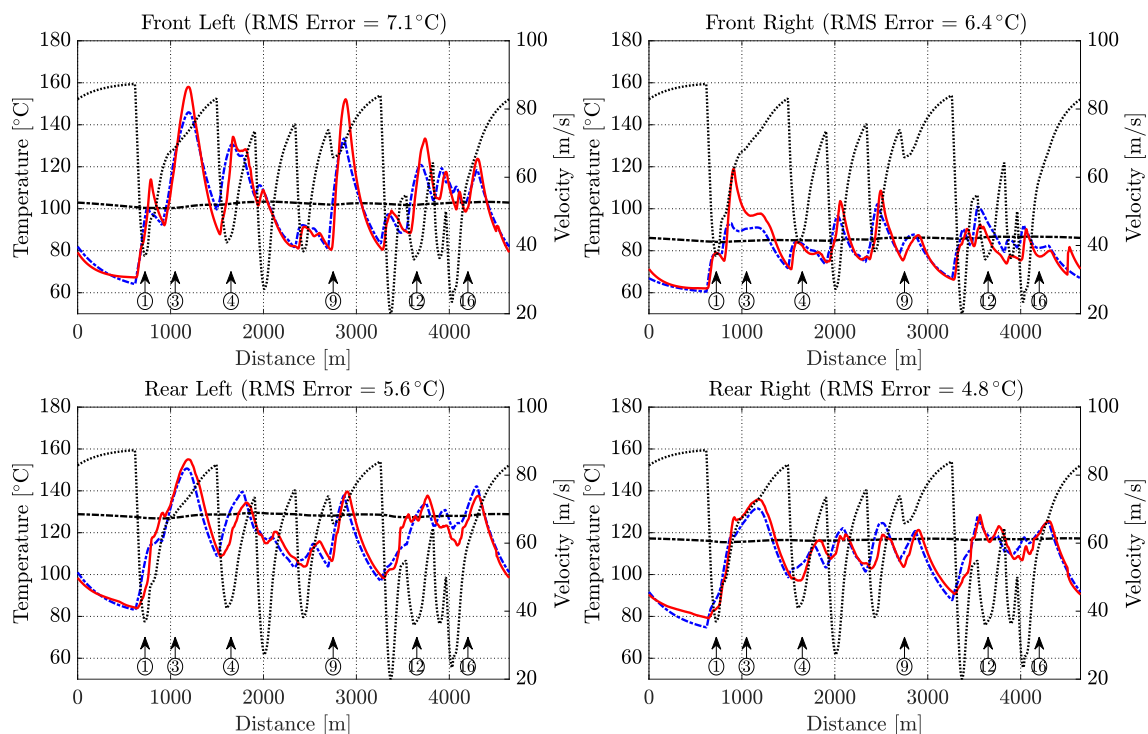
Figure 3.11. Tread and carcass temperature. Car speed (dotted), tread temperature telemetry data (red), model tread temperature (blue), model carcass temperature (dot-dash); the locations of some corners circled.
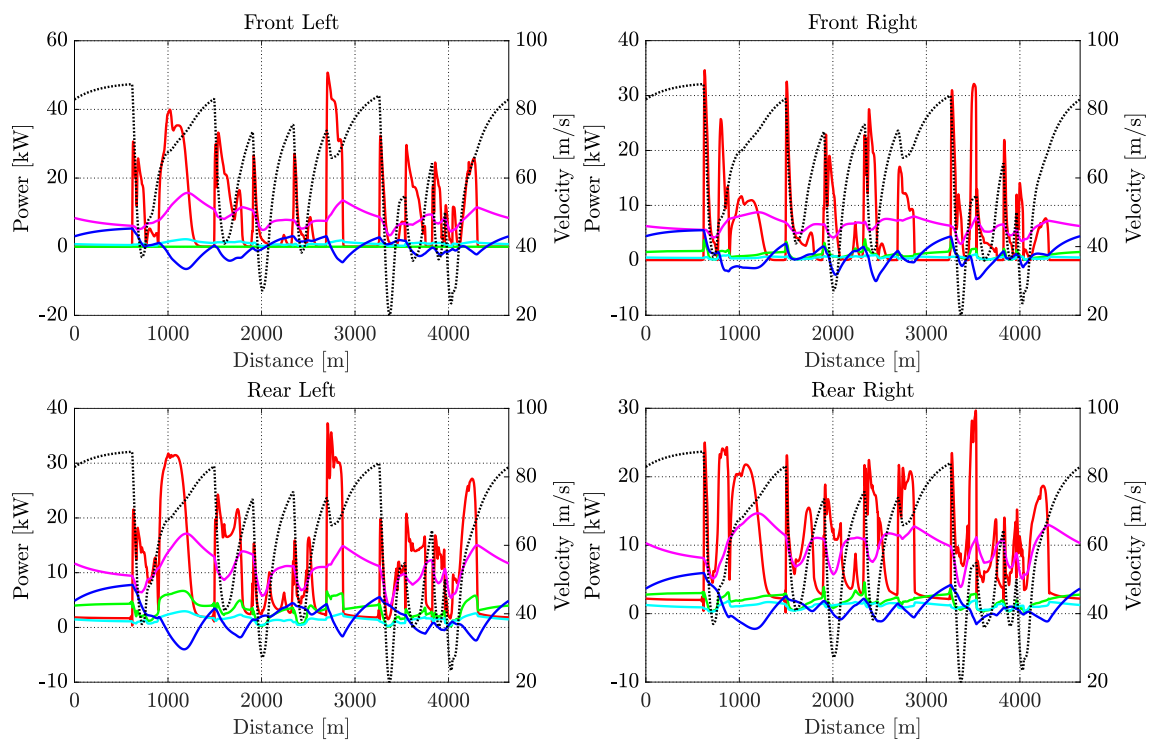
Figure 3.12. Heat flows. The car speed (dotted), Q_1 (red), Q_2 (green); Q_3 (magenta); Q_4 (cyan); Q_5 (blue).

3.4.4 Tyre wear model

The model developed in [14] forms the basis of this aspect of the work. The wear rate ($\dot{w}$) is added as an extra state to be associated with each tyre, so that the total tyre wear can be calculated and restricted as part of the optimal control problem. The mechanical abrasion between a tyre and track asperities is modelled using the power law relationship:

$$\dot{w}_p = w_{p1}\left(\frac{Q_1}{Q_{ref}}\right)^{w_{p2}},\tag{3.85}$$

where Q_1 is given in (3.69), and w_{p1}, w_{p2} and Q_{ref} are constants; see Table B.4.

If a tyre is overworked while cold, particles break away from the surface in a phenomenon known as graining, which is modelled by:

$$\dot{w}_g = w_{g1}\big(\max(T_{tp} - T_{tr}, 0)\big)^{w_{g2}};\tag{3.86}$$

where w_{g1} and w_{g2} are constants; see Table B.4. The wear transition temperature T_{tp} is in the optimal grip temperature range; see Figure 3.14.

If a tyre gets too hot, local hot spots will form leading to more extreme tyre wear. This phenomenon is called blistering and is modelled by:

$$\dot{w}_b = w_{b1}(\max(T_{tr} - T_{tp}, 0))^{w_{b2}}, \tag{3.87}$$

where w_{b1} and w_{b2} are constants.

As is apparent from (3.86) and (3.87), these wear mechanisms occur either side of the transition temperature. In combination they represent the 'two-mechanism' abrasion that occur either side of the optimal operating temperature.

Most optimal control solvers using non-linear programmes cannot deal with 'non-smooth' functions. To that end, smooth approximations for (3.86) and (3.87) are given in [42]:

$$\dot{w}_g = w_{g1}\left((T_{tp} - T_{tr} + \sqrt{(T_{tp} - T_{tr})^2 + \varepsilon})/2\right)^{w_{g2}} \tag{3.88}$$

$$\dot{w}_b = w_{b1}\left((T_{tr} - T_{tp} + \sqrt{(T_{tr} - T_{tp})^2 + \varepsilon})/2\right)^{w_{b2}} \tag{3.89}$$

The total tyre wear is found by integrating the superposition of the three wear rate mechanisms given in (3.85), (3.86) and (3.87). The combined wear rate is illustrated in Figure 3.13.
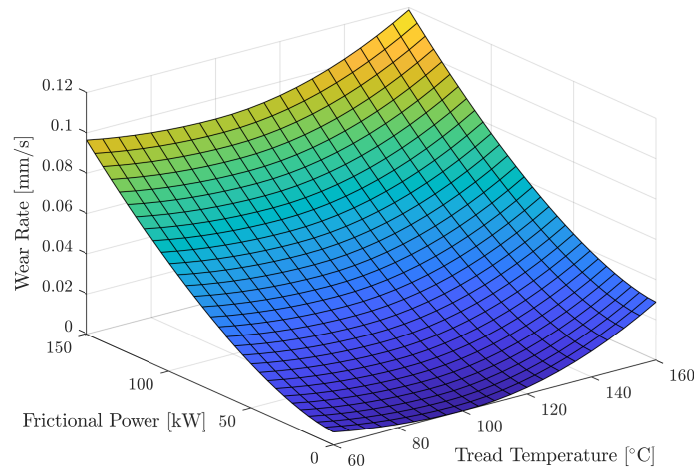
Figure 3.13. Wear rate shown as a function of frictional power and tread temperature (taken from [14], with permission).

3.4.5   Performance altering components

Tyre degradation has a negative impact on race performance and is needs to be included in the optimal control problem. Both temperature and wear characteristics will be considered.

3.4.5.1   Temperature-grip sensitivity

The temperature window in which the maximum achievable grip is obtained is shown in Figure 3.14; this curve is representative of a super-soft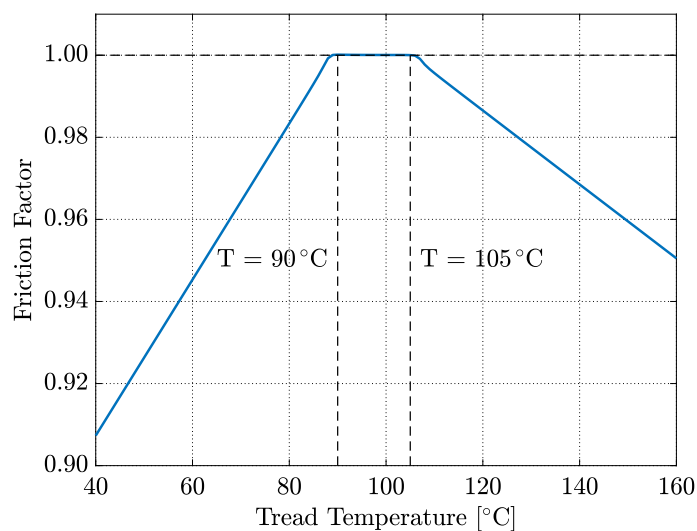 tyre (the compound that will be used for the simulations in the following sections). This window must be adjusted for each tyre compound. The aim is to get the tyre surface temperatures into this optimal operating window and hold it there as nearly as possible. In this case optimal grip is achieved when the tread temperature lies between 90 °C and 105 °C.

Figure 3.14. Optimal temperature window for super-soft tyre compound.

The tread-only model used in [14] is limited by the fact that it exaggerates the extent to which it is possible to cool the tread once it overheats. If one wants to reduce the temperature of an over-heated tread, one has to reduce the temperature of the tyre carcass—this process is slowed by the relatively high thermal inertia of the carcass as compared to that of the tyre tread. It is thus important to introduce a carcass temperature state that represents this thermal-inertia-related lag. In a typical race the tread will undergo rapid temperature variations throughout a racing lap, while the carcass temperature varies more slowly. Once the carcass has overheated, cooling it down again is a slower process.

3.4.5.2   Wear-grip sensitivity

Tyre tread temperature variations are reversible effects. In contrast, tyre wear is not—once a tyre is worn out it stays worn out! It is therefore necessary to include in the tyre model a mechanism that recognises the irreversible degradation resulting from wear.

Figure 2.8 shows how the handling performance of different tyres degrade over their lifetime. This figure was originally published in [34] and reports that racing tyres have an approximate usable range of 80 km. It is assumed that that at zero distance travelled, a tyre has maximum tread depth and at the end of its usable range zero tread remains. The curve for a racing tyre has been normalised so that the maximum available grip is equal to unity, and the units of the x-axis have been changed to represent the fraction of the tyre's tread that has been lost due to wear so that the figure can be easily adapted for various tyre compounds. The resulting curve is given in Figure 3.15:
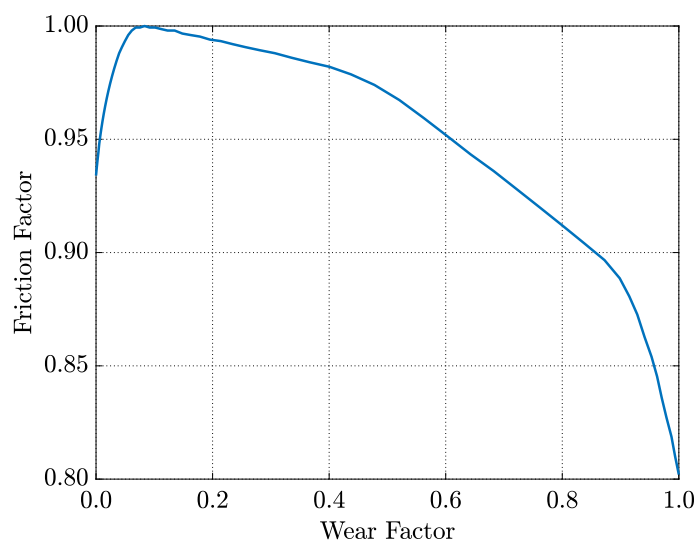
Figure 3.15. Wear characteristics of a racing tyre compound.

3.4.5.3   Combined temperature–wear characteristics

In order to complete the tyre model, we will combine the temperature-grip sensitivity curve with the wear-grip sensitivity curve given from the previous sections. This allows the tyre grip to be modelled as a function of the tread temperature (a reversible process), and tyre wear (an irreversible process). As a result, the tyres can be managed by the optimal control process until they can be replaced at scheduled pit stops. The three-dimensional grip-sensitivity curve used in this study is shown in Figure 3.16. Slices along constant wear planes resemble Figure 3.14, whereas slices along constant temperature planes resemble Figure 3.15.
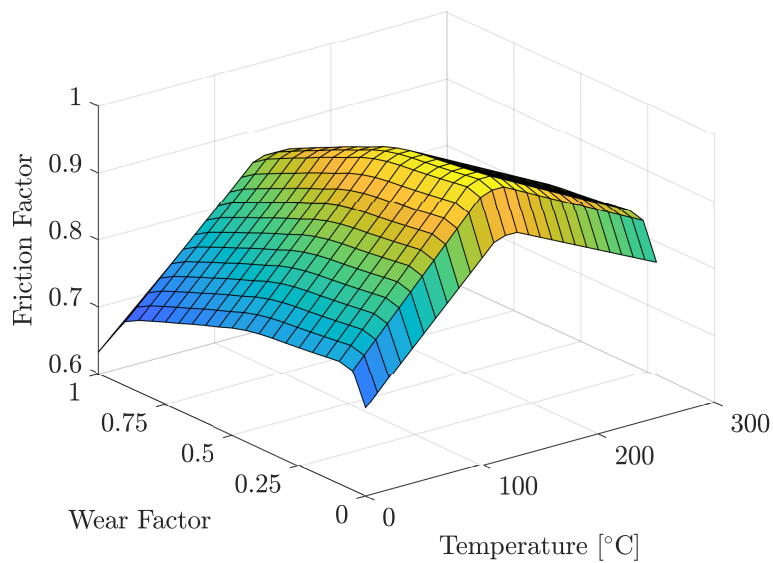
Figure 3.16. Combined temperature–wear grip curve.

3.5 OPTIMAL CONTROL PROBLEM FORMULATION

The model detailed in the sections above will be used to formulate the optimal control problem using the general Bolza form as discussed in Section 2.2.1.

3.5.1 Performance index

The objective for this work is to determine the optimal inputs that will allow a Formula One car to complete a set amount of laps around the Circuit de Catalunya in minimum time. The performance index for the system can be written as

$$J = \sum_{i=1}^{n} \int_{s_{0i}}^{s_{fi}} S_f \, ds, \tag{3.90}$$

where i represents the lap number, n the amount of laps over which the problem is solved, s_0 the distance at the starting point for lap number i and s_f the distance at the end of the lap number i.

3.5.2   State variables

The dynamic system has 22 state variables which are listed in the table below.

Table 3.2. System state variables

Parameter	Description
n	Lateral position of vehicle's centre of mass relative to track centre line
ξ	Angle between vehicle and track
u	Longitudinal component of vehicle's mass centre velocity
v	Lateral component of vehicle's mass centre velocity
ω	Vehicle yaw rate ($\dot{\psi}$)
δ	Steering angle
κ_{rr}	Longitudinal slip coefficient for rear-right wheel
κ_{rl}	Longitudinal slip coefficient for rear-left wheel
κ_{fr}	Longitudinal slip coefficient for front-right wheel
κ_{fl}	Longitudinal slip coefficient for front-left wheel
T_{tr_rr}	Tread temperature for rear-right wheel
T_{tr_rl}	Tread temperature for rear-left wheel
T_{tr_fr}	Tread temperature for front-right wheel
T_{tr_fl}	Tread temperature for front-left wheel
T_{ca_rr}	Carcass temperature for rear-right wheel
T_{ca_rl}	Carcass temperature for rear-left wheel
T_{ca_fr}	Carcass temperature for front-right wheel
T_{ca_fl}	Carcass temperature for front-left wheel
w_{T_rr}	Total wear for rear-right wheel
w_{T_rl}	Total wear for rear-left wheel
w_{T_fr}	Total wear for front-right wheel
w_{T_fl}	Total wear for front-left wheel

3.5.3   Control variables

The dynamic system has 9 input variables which are listed in the table below.

Table 3.3. System control inputs

Parameter	Description
$\dot{\delta}$	Rate of change in steering angle
$\dot{\kappa}_{rr}$	Rate of change in rear-right longitudinal slip coefficient
$\dot{\kappa}_{rl}$	Rate of change in rear-left longitudinal slip coefficient
$\dot{\kappa}_{fr}$	Rate of change in front-right longitudinal slip coefficient
$\dot{\kappa}_{fl}$	Rate of change in front-left longitudinal slip coefficient
F_{rrz}	Down force at rear-right wheel in z-direction
F_{rlz}	Down force at rear-left wheel in z-direction
F_{frz}	Down force at front-right wheel in z-direction
F_{flz}	Down force at front-left wheel in z-direction

3.5.4   Differential equations

Each one of the state variables has a corresponding differential equation that is integrated over the solution horizon (in our case over n laps). These equations were derived in the previous sections and are summarised below:

$$\frac{\mathrm{d}n}{\mathrm{d}s} = S_f(u\sin\xi + v\cos\xi) \tag{3.24}$$

$$\frac{\mathrm{d}\xi}{\mathrm{d}s} = S_f(\dot{\psi} - \mathcal{C}) \tag{3.25}$$

$$\frac{\mathrm{d}u}{\mathrm{d}s} = S_f\dot{u} \tag{3.32}$$

$$\frac{\mathrm{d}v}{\mathrm{d}s} = S_f\dot{v} \tag{3.33}$$

$$\frac{\mathrm{d}\omega}{\mathrm{d}s} = S_f(s)\dot{\omega} \tag{3.34}$$

$$\frac{\mathrm{d}\delta}{\mathrm{d}s} = S_f\dot{\delta} \tag{Table 3.3}$$

$$\frac{\mathrm{d}\kappa_{rr}}{\mathrm{d}s} = S_f\dot{\kappa}_{rr} \tag{Table 3.3}$$

$$\frac{\mathrm{d}\kappa_{rl}}{\mathrm{d}s} = S_f\dot{\kappa}_{rl} \tag{Table 3.3}$$

$$\frac{d\kappa_{fr}}{ds} = S_f \dot{\kappa}_{fr} \qquad \text{(Table 3.3)}$$

$$\frac{d\kappa_{fl}}{ds} = S_f \dot{\kappa}_{fl} \qquad \text{(Table 3.3)}$$

$$\frac{dT_{tr\_rr}}{ds} = S_f \left(\frac{Q1 - Q3 - Q4 + Q5}{m_t\, c_t} \right)_{rr} \qquad (3.67)$$

$$\frac{dT_{tr\_rl}}{ds} = S_f \left(\frac{Q1 - Q3 - Q4 + Q5}{m_t\, c_t} \right)_{rl} \qquad (3.67)$$

$$\frac{dT_{tr\_fr}}{ds} = S_f \left(\frac{Q1 - Q3 - Q4 + Q5}{m_t\, c_t} \right)_{fr} \qquad (3.67)$$

$$\frac{dT_{tr\_fl}}{ds} = S_f \left(\frac{Q1 - Q3 - Q4 + Q5}{m_t\, c_t} \right)_{fl} \qquad (3.67)$$

$$\frac{dT_{ca\_rr}}{ds} = S_f (Q2 - Q5)_{rr} \qquad (3.68)$$

$$\frac{dT_{ca\_rl}}{ds} = S_f (Q2 - Q5)_{rl} \qquad (3.68)$$

$$\frac{dT_{ca\_fr}}{ds} = S_f (Q2 - Q5)_{fr} \qquad (3.68)$$

$$\frac{dT_{ca\_fl}}{ds} = S_f (Q2 - Q5)_{fl}. \qquad (3.68)$$

3.5.5 Path constraints

The algebraic equations derived in the previous sections constitute the equality constraints for the optimisation problem. The equations with their original references are summarised below:

$$0 = w_r(F_{rlz} - F_{rrz}) + w_f(F_{flz} - F_{frz}) + hF_y \qquad (3.35)$$

$$0 = b(F_{rrz} + F_{rlz}) - a(F_{frz} + F_{flz}) + hF_x + (a_A - a)F_{az} \qquad (3.36)$$

$$0 = F_{rrz} + F_{rlz} + F_{frz} + F_{flz} + Mg + F_{az} \qquad (3.37)$$

$$0 = F_{frz} - F_{flz} - D_{roll}(F_{frz} + F_{rrz} - F_{flz} - F_{rlz}) \qquad (3.38)$$

$$0 = \max(\omega_{fr}, 0)\max(\omega_{fl}, 0)(F_{frx} - F_{flx}) \qquad (3.41)$$

$$0 = R(F_{lrx} - F_{rrx}) - k_d(\omega_{rl} - \omega_{rr}). \qquad (3.42)$$

The system has one inequality constraint limiting the torque delivered to the rear axle:

$$u(F_{rrx} + F_{rlx}) \le P_{\max}. \qquad (3.31)$$

In addition to the constraints listed above, each wheel must also be prohibited to exceed the track boundaries:

$$0 = n - w_f \cos(\xi) + a \sin(\xi) - T_{lb} \tag{3.91}$$

$$0 = n - w_r \cos(\xi) - b \sin(\xi) - T_{lb} \tag{3.92}$$

$$0 = T_{rb} - n - w_f \cos(\xi) - a \sin(\xi) \tag{3.93}$$

$$0 = T_{rb} - n - w_r \cos(\xi) + b \sin(\xi), \tag{3.94}$$

where T_{lb} and T_{rb} are the left and right track boundaries respectively and the parameters a, b, w_f and w_r are defined in Figure 3.5.

3.5.6   Boundary conditions

A number of simulations have been designed to test the significance of various aspects of the model that has been derived in the previous sections. The boundary conditions for each simulation is unique and will be discussed in the next chapter.

CHAPTER 4   RESULTS AND DISCUSSION

4.1   CHAPTER OVERVIEW

Various simulations have been designed to investigate the effect that each modification to the model has on system dynamics and to explore its influence on tyre management. This has been done by omitting certain dynamic features of the model and by tailoring the initial conditions and objective function of the optimal control problem. The setup of each simulation will be discussed first followed by the results.

Thermal influences will be studied in isolation first, with the effect of wear considered thereafter. This is followed by a sensitivity study that was performed to investigate the effect of track temperature on racing performance. We conclude with some track-side observations.

4.2   SIMULATION SETUP

4.2.1   Tyre starting temperature and compound

Racing teams use tyre blankets during a race to ensure that the tyres are within the optimal temperature band as soon as the car enters the track. Each simulation that will follow has the starting temperature of both the tyre tread and carcass fixed at 60 °C. This ensures that the tyres start the simulation at a suboptimal temperature, which will force the solver to warm the tyres so that optimal grip can be obtained. A super-soft compound is used that will achieve optimal grip when the tread temperature is between 90 °C and 105 °C; refer to Figure 3.14.

4.2.2 Simulation 1: Effect of adding carcass temperature

The optimal control solver is used to minimise the time taken to complete fifteen laps around the Circuit de Catalunya in Barcelona. For this simulation wear has been excluded from the model to focus on the dynamic effects that the carcass temperature has on the OCP. It is expected that the carcass will take longer to reach its optimal temperature (relative to the tread) due to its greater thermal inertia.

4.2.3 Simulation 2: Effect of adding tyre wear

Wear dynamics have been added for this simulation. Time will be minimised for a single lap using various wear rates. The model has been adapted for each run by multiplying the nominal wear rate with a factor so that the extent to which a tyre is worn can be exaggerated. This will reduce the available grip and consequently lead to slower lap times.

4.2.4 Simulation 3: Multi-lap simulation

Now that the two new additions to the model (modelling carcass temperature and grip as a function of tyre wear) has been considered in isolation, they can be used together to evaluate race performance over multiple laps. Wear parameters were adjusted back to their nominal values after which the optimal control solver has been used to minimise the time taken to complete fifteen laps. The aim of this simulation is to investigate how performance degrades over a racing stint (as opposed to a single lap) and to determine if a tyre management strategy can be optimised by means of computer simulation.

4.2.5 Simulation 4: Track temperature sensitivity study

The concluding simulation illustrates the effect of track temperature variations on the car and tyre performance. The first lap has no minimum-completion-time objective, and is used to 'scrub in' the tyres and bring them up to their operating temperature. The initial tyre temperatures were fixed at 60 °C, with the starting speed set at 22.2 m/s or 80 km/h (a representative pit lane exit speed). The second lap is a racing lap in which the lap time is minimised. This simulation was repeated for track temperatures ranging from 0 °C to 50 °C, with the ambient temperature held constant at 25 °C.

4.3   SIMULATION RESULTS

The general-purpose optimal control problem solver GPOPS-II [3] is used to perform the optimal control calculations for each simulation detailed in the previous section.
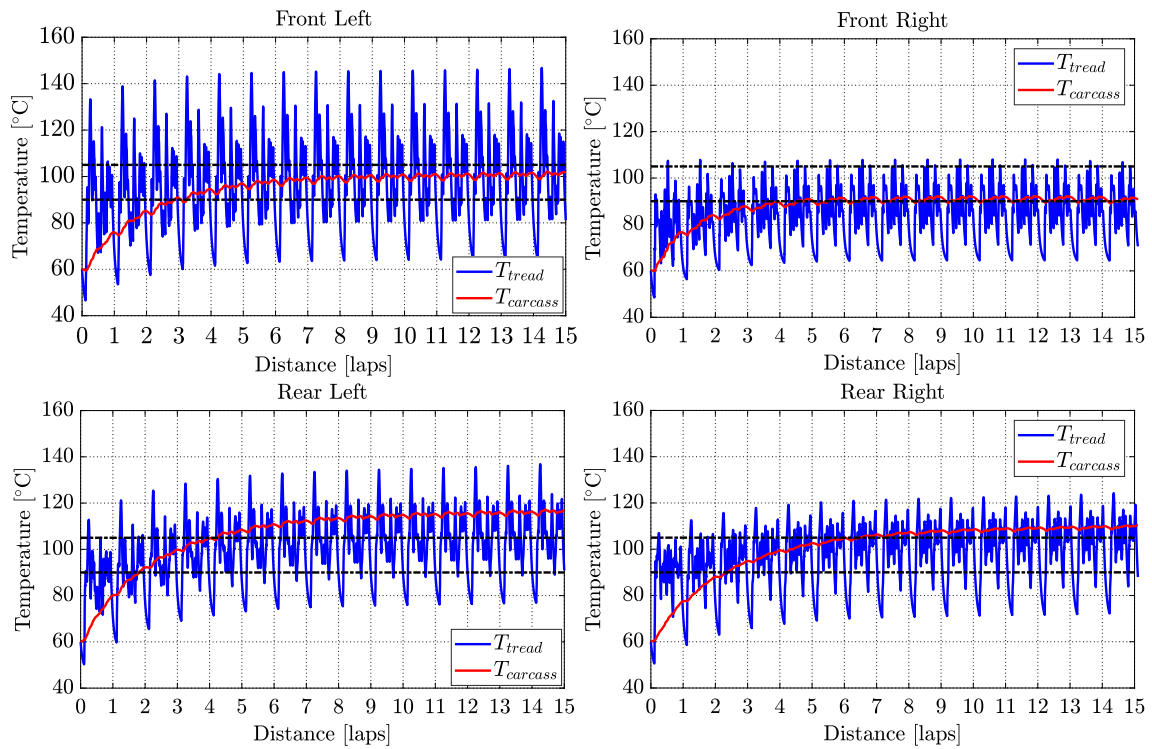
4.3.1   Simulation 1: Effect of adding carcass temperature

Figure 4.1 shows the temperature profiles of each tyre with the optimal temperature window indicated by the dash-dotted black lines. Figure 4.2 shows the recorded lap times for each lap. As one would expect, the first lap is a relatively slow lap, because the tyres are cold and thus unable to provide optimal grip. In the second lap the tread temperatures increase into their optimal operating range. This is not the case for the front right tyre, which is still running too cool. Despite this, the second lap is the fastest lap with a lap time of 81.07 s.

The tread temperature reacts rapidly to inputs such braking, cornering and acceleration whereas the carcass temperature slowly increases with time. Figure 4.1 shows that the tread temperature "cycles" around the carcass temperature as it reacts to the driver inputs, with the average temperature being approximately equal to that of the carcass. The consequence of this is that average tread temperature increases alongside the carcass, making it more difficult to keep the tread temperature within the optimal window.

The positive time deltas in Figure 4.2 represent laps that were slower than lap two. This is a result of sub-optimal tread temperatures that cannot provide maximum grip due to an overheating carcass. The time for Lap 10 increases to 81.17 s, which is only slightly faster than the cold-tyre first lap. The penalty in lap time eventually settles out at 0.11 s when the carcasses reach a steady-state.

It has been shown that the optimal control solver tries to maximise the time during which the tread temperatures are within the optimal window. In doing so grip is maximised which reduces lap time. The carcass however cannot be managed to stay within this window; three of the tyres had stead-state temperatures outside of the optimal window. In the absence of carcass temperature modelling, the identical lap times would be achieved once the tyres are heated up into the desired temperature window.

Figure 4.1. Temperature profiles for each tyre during simulation 1.
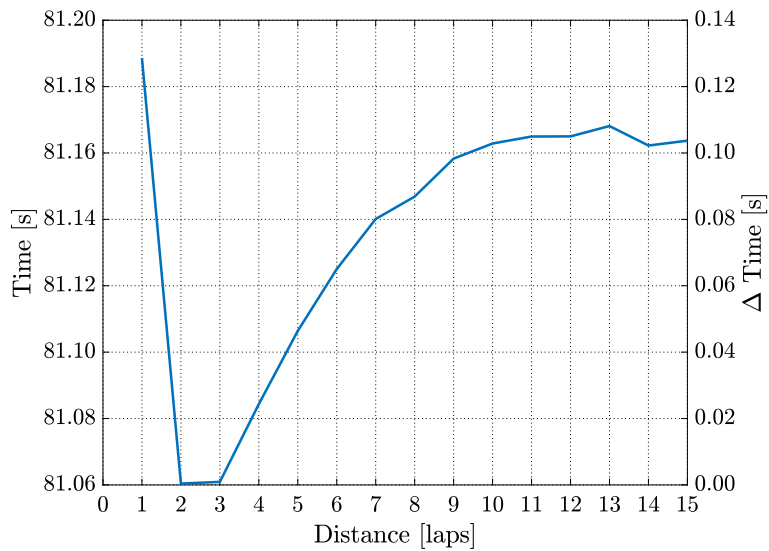

Figure 4.2. Lap times are shown on the left axis, with the time difference relative to the fastest lap shown on the right axis.

4.3.2   Simulation 2: Effect of tyre wear

Figure 4.3 shows the temperature profiles of each tyre with the optimal temperature window indicated by the dash-dotted black lines. Figure 4.4 shows the velocity profile associated with each wear rate and Figure 4.5 shows the wear profiles for each tyre.

Although all the tyre carcasses remain below the optimal operating temperature range for the entire lap, the tyre treads are within their optimal range after 750 m (with the exception of the front-right tyre, as was the case with the first simulation). The car was able to start a lap at full speed for the nominal case only; this is evident in the tread temperature that cools down during the first 500 m of the lap as a result of convection with ambient air on the main straight. In the cases with exaggerated wear however, emphasis is placed on getting the tread warmed up instead. The peaks of the tread temperature curves are also reduced with increasing severity in wear rate; this happens because grip is permanently reduced with tyre wear (see Figure 3.15) and overheating the tread will accelerate this process (see Figure 3.13).
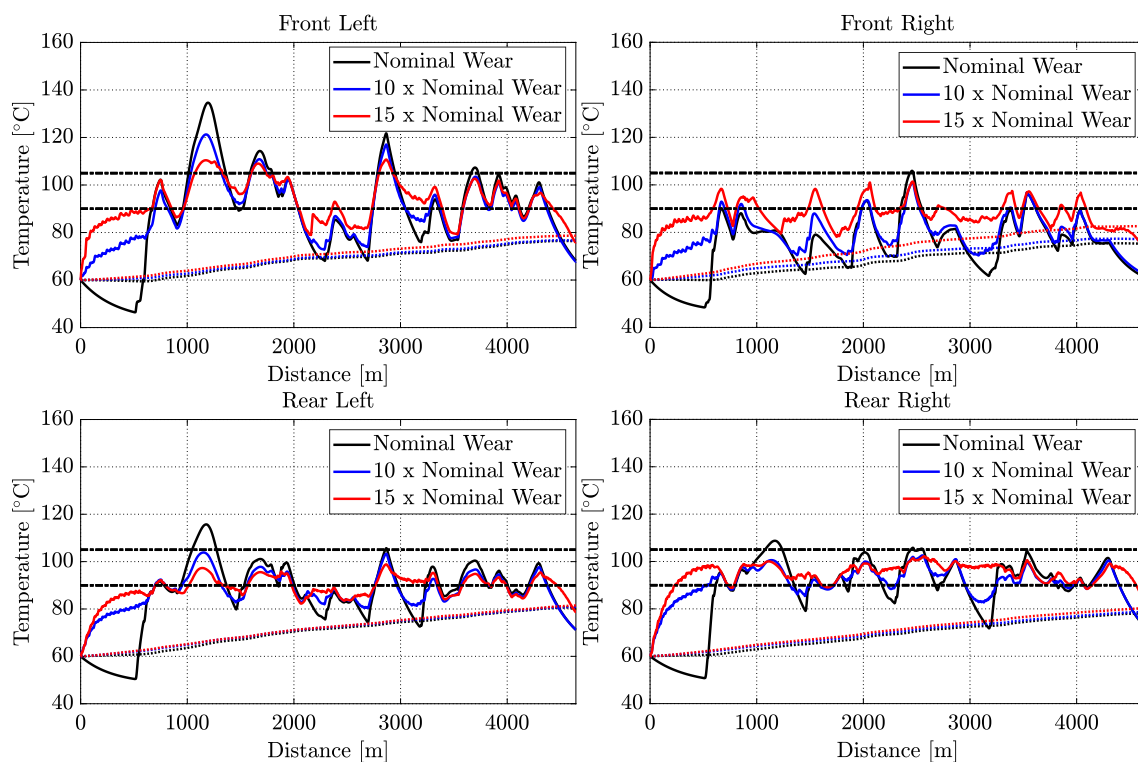
Figure 4.3. Tread temperatures (solid) and carcass temperatures (dotted) for simulation 2.

As is shown in Figure 4.4, the vehicle speed is fastest in the no-wear reference case. Small speed reductions are observed in the nominal wear and ×10 nominal wear cases. These speed reductions are accompanied by slightly earlier braking, and slightly lower cornering speeds. When the wear is increased to 15 times the nominal wear rate however, the race speeds fall away significantly and the car becomes uncompetitive.
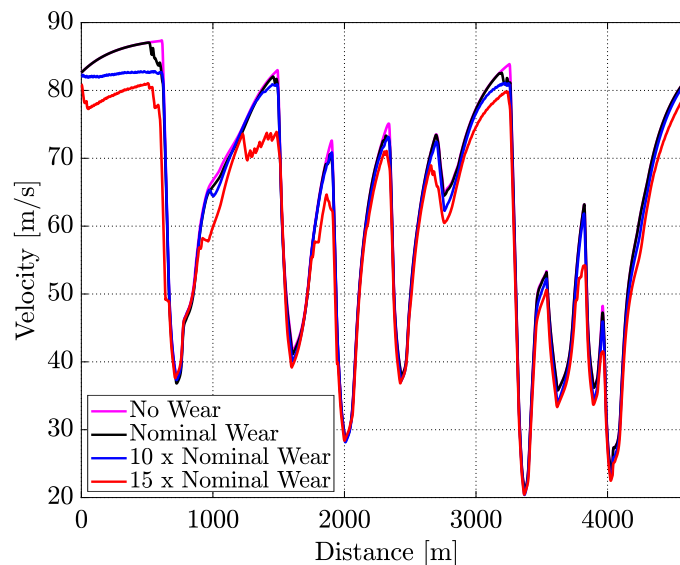
Figure 4.4. Vehicle speed for each wear rate in simulation 2.

The reason for this significant drop in performance is evident in Figure 4.5, which shows that in the ×15 nominal case, despite optimal tyre management, both front tyres are completely worn out by the end of the lap (the new tread is assumed to be 5 mm thick). In the ×10 nominal case the front tyres are heavily worn, but this has not as yet had a catastrophic effect on the car's performance.

4.3.3   Simulation 3: Multi-lap simulation

In this simulation the tyre wear model was adjusted to its nominal parameters to allow multiple laps to be completed without premature tyre degradation. Figure 4.6 shows the temperature profiles of each tyre with the optimal temperature window indicated by the dash-dotted black lines. Figure 4.8 (a) shows the grip profiles for each tyre, with friction plotted as solid lines and wear plotted as dotted lines. Figure 4.8 (b) shows the recorded lap times for each lap and Figure 4.7 shows the heat flows through each tyre.
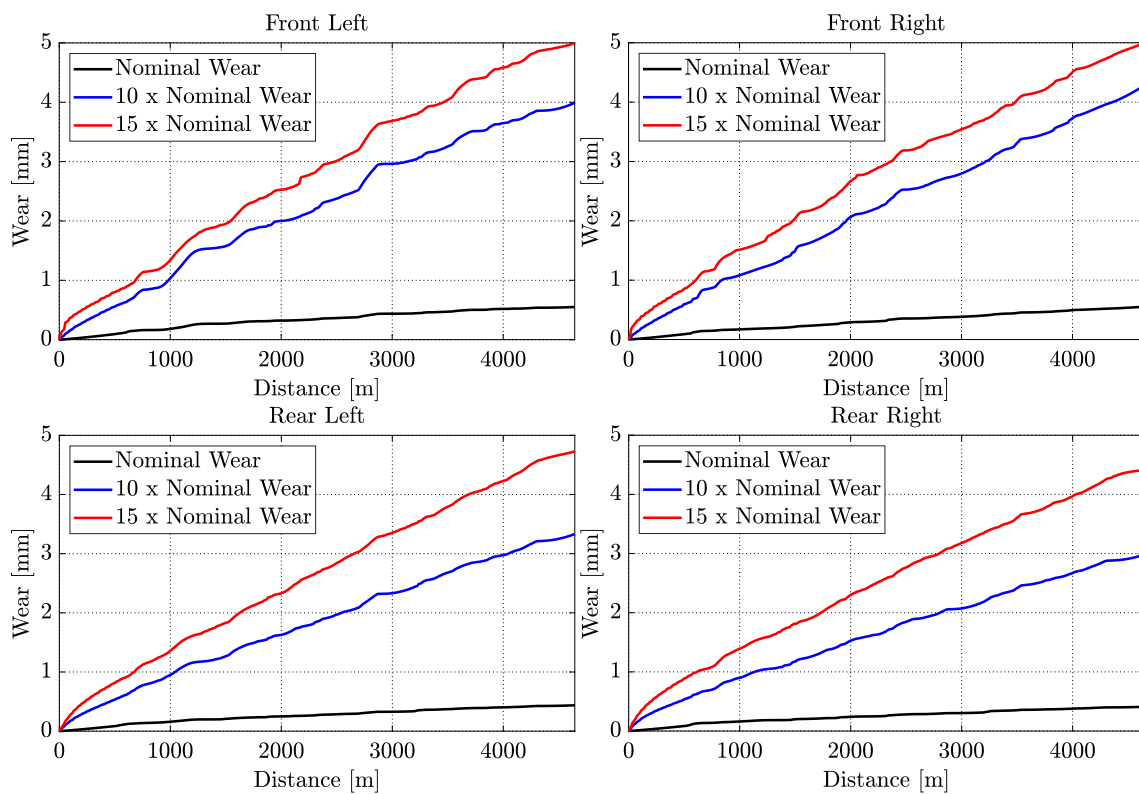
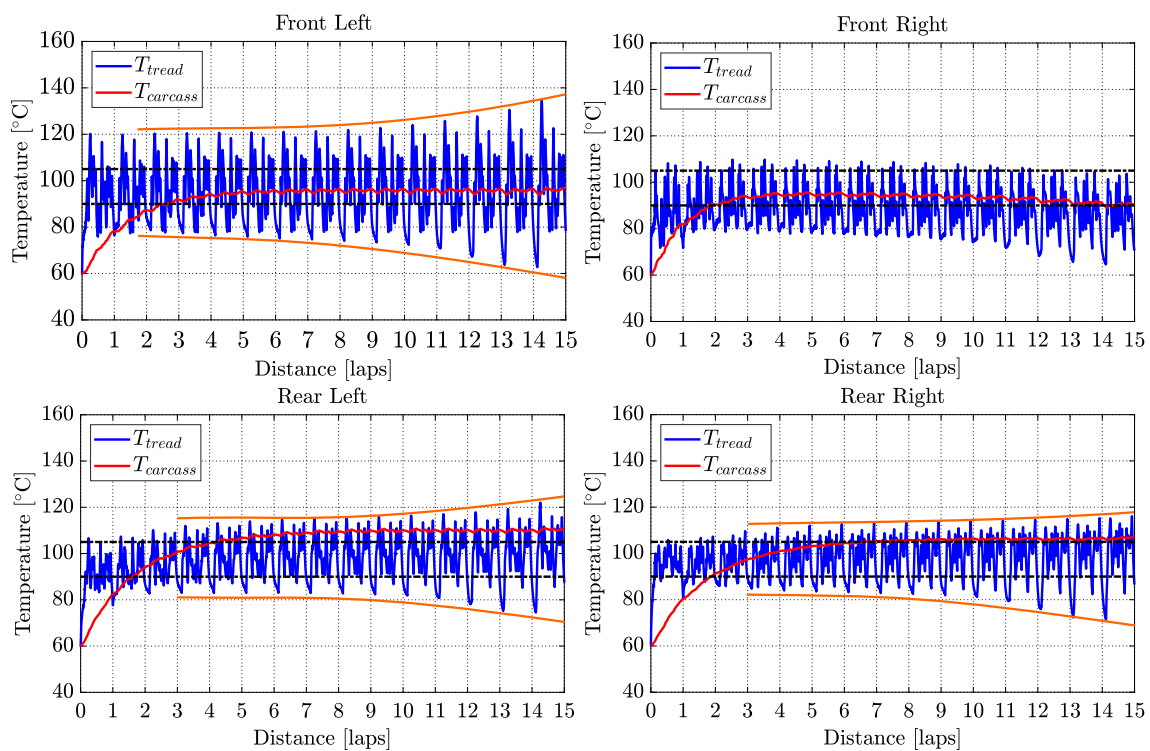**Figure 4.5.** Total wear for each wear rate in simulation 2.

Figure 4.6. Temperature profiles for each tyre during simulation 3.

The carcass temperatures once again reach a steady-state in a similar fashion to the first simulation. In contrast to simulation 1 (which did not take account of wear effects) the tread temperature does not maintain a constant oscillation about the carcass temperature. Instead a "funnel" effect is observed where the peaks of the tread temperatures become larger as the tyres get worn (this is indicated by the orange lines in Figure 4.6).

The other difference when compared to the first simulation is that the carcass of the front right tyre starts to cool down after lap eight. Closer inspection of the heat flows in Figure 4.7 reveals that the average heat generated due to friction for each lap is the highest in lap one (to warm the tyres into the optimal band) after which is decays to a steady state after lap six. This is not the case for the front right tyre, whose average heat generated by friction, Q_1 starts decreasing again after lap eight which causes the carcass temperature to cool down.
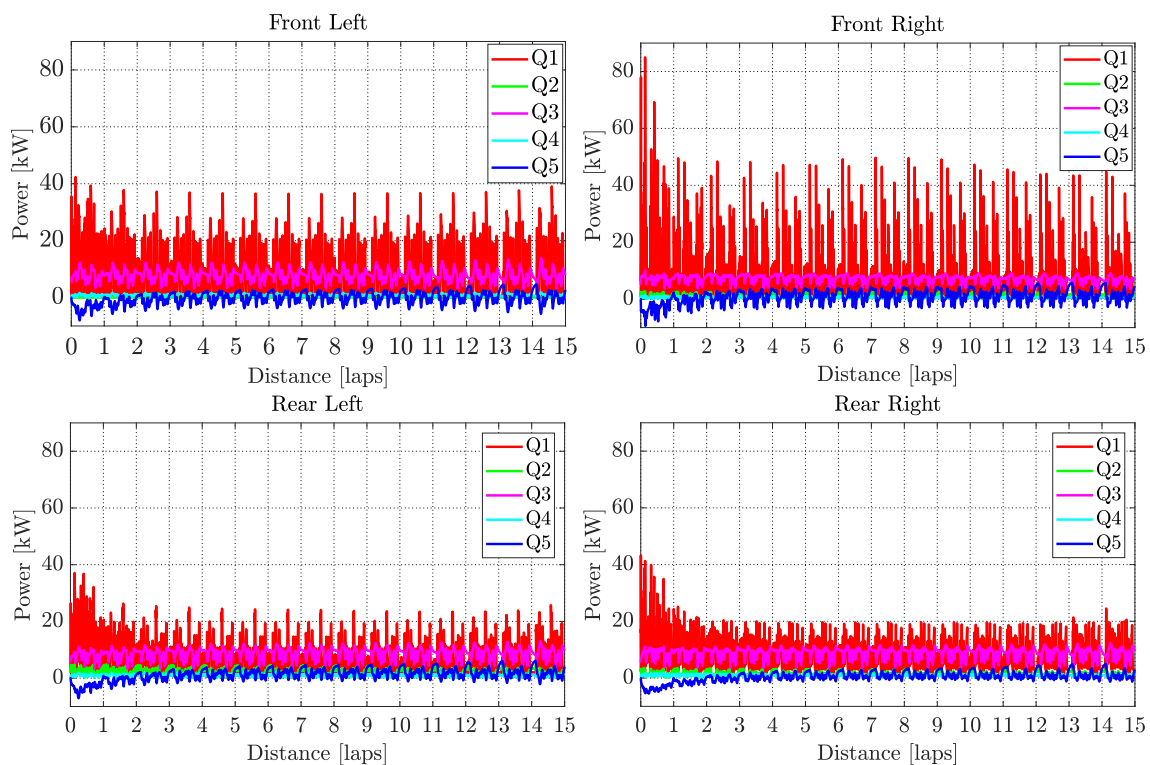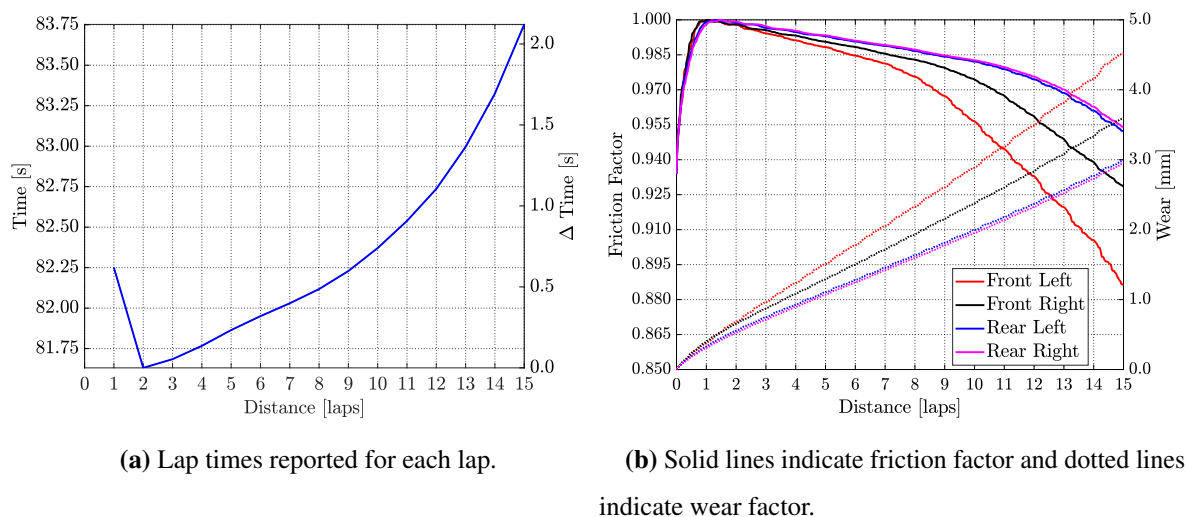

Figure 4.7. Heat flows through each tyre during simulation 3.

Lap two is once again the fastest lap. The slow first lap reflects the combined influence of cold new tyres that have not yet been 'rubbed in'. The tyres operate optimally between laps two and eight, with the lap times gradually increasing due to wear. After lap eight, tyre wear affects performance more

noticeably, and the lap times start to degrade. At some point in the stint, this drop-off in performance increases to the extent that the car is no longer competitive and a tyre change is required.

This performance drop-off is not seen in Figure 4.2, where tyre wear is unaccounted for, and the ΔT value reaches a steady-state value of approximately 0.1 s. When wear is accounted for, the lap ΔT continues to increase until the car is uncompetitive; see Figure 4.8(a). Figure 4.8(b) shows that the friction factor increases rapidly in the first lap when the tyres are being 'rubbed in'. After that they continue to wear with an accompanying reduction in the available friction. This wear-related degradation is most evident in the front-left tyre, which is down to 0.5 mm of tread at the end of the 15-lap stint. The front-right tyre is also well worn after 15 laps, with some life remaining in the rear tyres (approximately 2 mm of tread).

(a) Lap times reported for each lap.

(b) Solid lines indicate friction factor and dotted lines indicate wear factor.

Figure 4.8. Lap times (left) and grip curves (right) for simulation 3.

4.3.4   Simulation 4: Track temperature sensitivity study

The concluding simulation illustrates the influence of track temperature variations on tyre performance. Figure 4.9 (a) shows the velocity profile and Figure 4.9 (b) the friction/wear curves for a two lap simulation in which the track temperature was held constant at 10 °C. Figure 4.10 shows the temperature profiles of each tyre for various track temperatures with the optimal temperature window indicated by the dash-dotted black lines. Figure 4.11 shows the difference in wear of each tyre relative to the tyre that is worn most out of each one of the sensitivity simulations.

The first lap is used to 'rub in' the tyres so that lap two can start with optimal grip. The tyres are only worn enough to reach the peak of the grip curve. Figure 4.9 (b) shows that the friction factor is nearly unity for all four tyres at the start of the second lap. If lap one is completed at normal racing speeds, the tyres would be worn beyond the peak of the grip curve and as a result the majority of the first lap is completed at a reduced velocity less than 50 m/s.

(a) Car speed.

(b) Friction and wear factors.
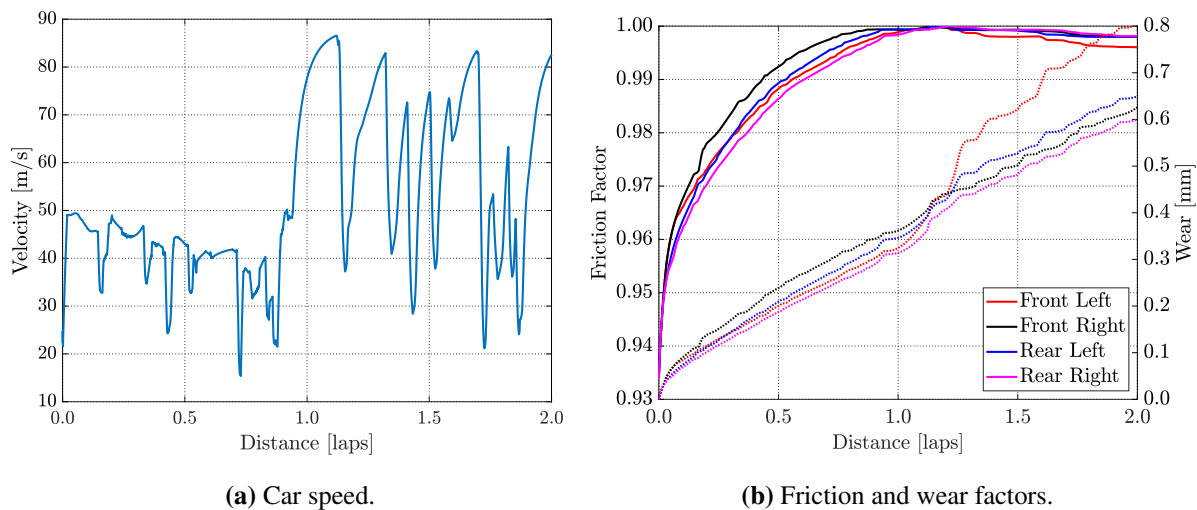
Figure 4.9. Speed, and friction and wear factors for an ambient temperature of 25 °C and a track temperature of 10 °C.

Figure 4.10 shows that the tread temperatures rise quickly and are within the optimal operating band within a quarter of a lap. The carcass temperatures rise more slowly, but are close to their operating temperatures by the end of the warm-up lap. A marginal increase in the tread temperature and a marginal reduction in carcass temperature is observed on the second lap with increasing track temperatures. This is predominantly the result of lower conduction losses to the track.

Tyre wear on the other hand increases as the track cools down. Figure 4.11 shows that the total wear for the 50 °C track temperature case is ≈ 0.67 mm at the rear left tyre; see the orange dotted reference curve. The remaining curves in Figure 4.11 show that as the track temperature drops, the tyre tread wear increases by up to 0.06 mm in the 0 °C case (also for the rear left tyre).
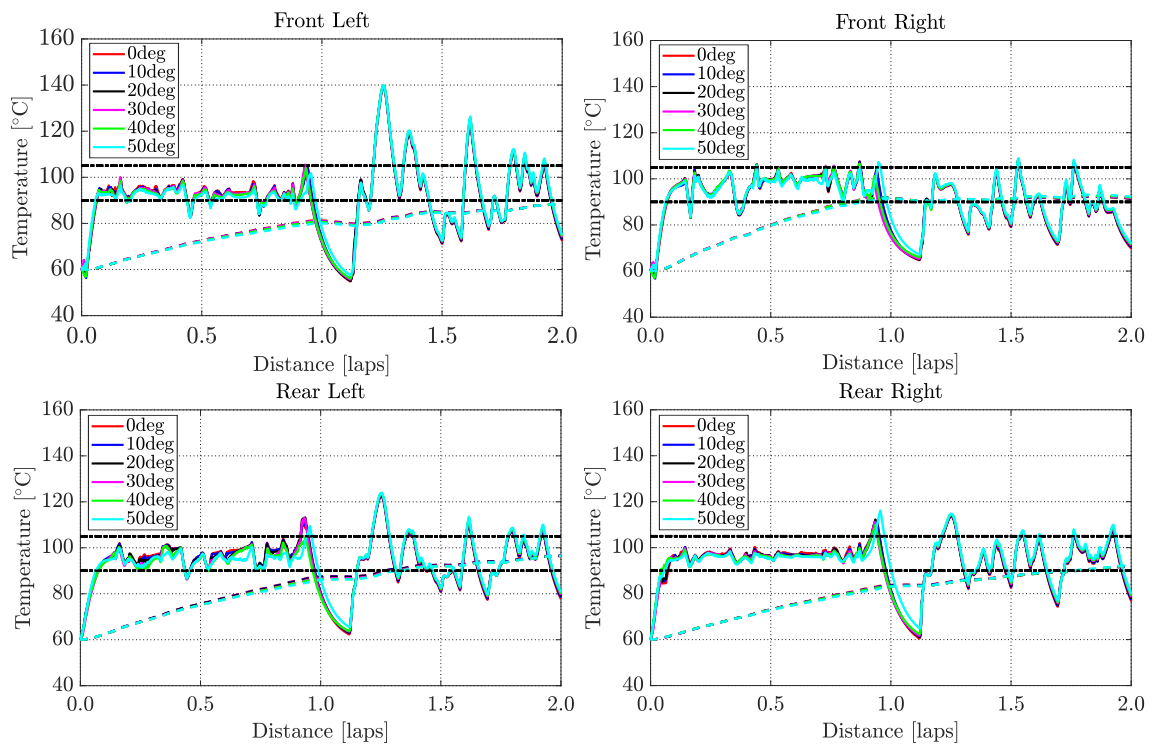
Figure 4.10. Temperature profiles for each tyre during simulation 4.
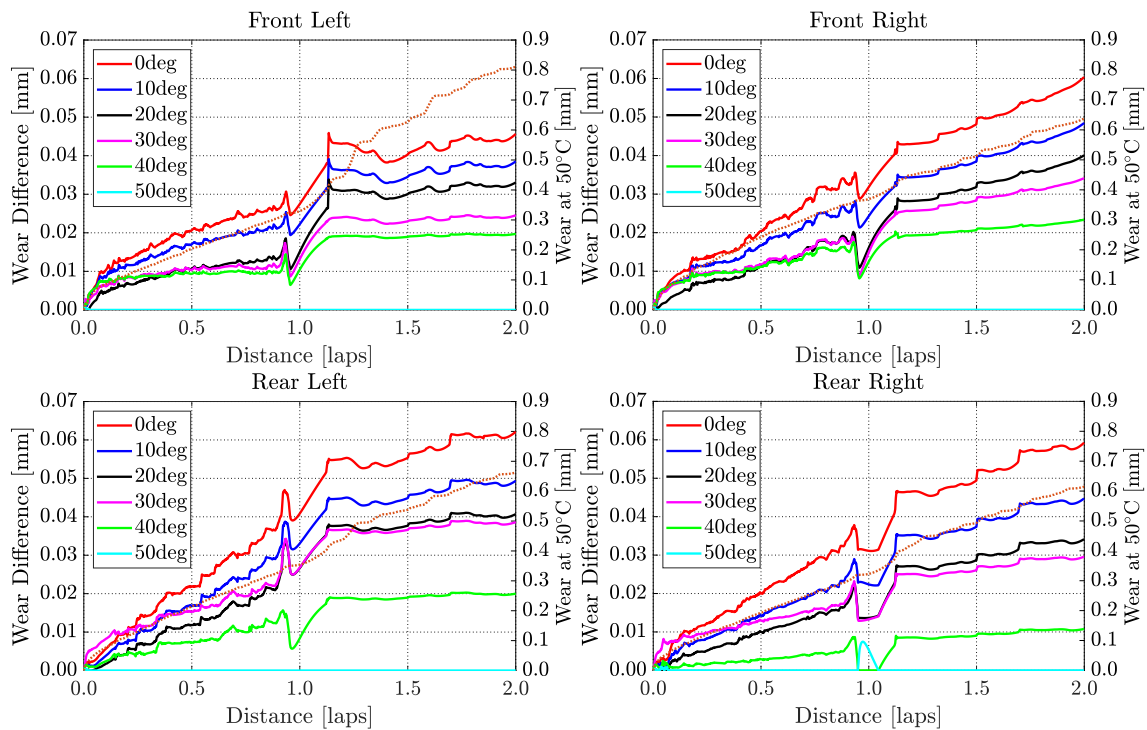
Figure 4.11. Wear difference for each tyre.

More heat is lost to the track due to the larger driving forces for conduction. This heat has to be made up elsewhere, by means of friction and deflection in the carcass, to ensure the tyres remain in the optimal temperature window. This accelerates tyre wear. Figure 3.13 also shows that tyre wear is a minimum at the graining-blistering transition temperature (of 100 °C in this case). A cooler track will therefore drive the tread temperature further away from the minimum point, which inherently causes more wear.

4.3.5   Practical example

Tyre wear and carcass temperature influences are vital in the development of a practical tyre management strategy. On 8 September 2019, Charles Leclerc claimed victory for Ferrari in the Italian Grand Prix. Charles Leclerc, Lewis Hamilton and Valtteri Bottas battled for the top three positions throughout the race. All three drivers started the race on the soft compound tyres, but opted for different strategies after their respective pit stops. The time difference for each driver relative to the leader of the race is shown in Figure 4.12.

Mercedes implemented two different strategies: (i) they pitted Hamilton nine laps before Bottas and fitted medium compound tyres; (ii) they pitted Bottas much later so that he would finish the race on fresher tyres. Ferrari pitted Leclerc immediately after Hamilton, but opted for hard compound tyres.

A combination of Ferrari's straight-line speed advantage, and knowledge of the tyre wear/performance characteristics helped them to victory. By lap forty one Hamilton's tyres had reached the end of their life, and at this point he traded places with Bottas (who was on fresher tyres). After lap twenty eight the gap between Bottas and Leclerc continued to decrease, because the medium compound tyres fitted to Bottas' car were faster (and newer) than the hard compound tyres on Leclerc's Ferrari. Ferrari's strategy to go for a harder compound put them in a position to compete for a world championship that would not have been otherwise possible.
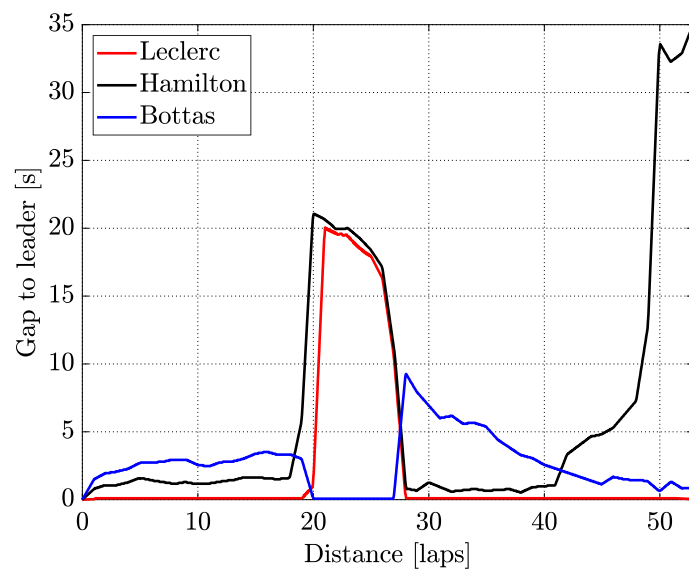
Figure 4.12. Gap to the race leader of the 2019 Italy Grand Prix—data accessed from [47].

CHAPTER 5   CONCLUSION

A thermodynamic tyre model is presented in which the tread and carcass temperatures are represented. The tyres' thermal behaviour impacts directly on their grip and wear properties; both are optimal within a narrow range of temperature. As the tyre wears, the peak friction reduces–the introduction of this wear-related grip feature is one of the novelties of this research. The tread temperature reacts rapidly to driver inputs and can be manipulated relatively easily into the optimal temperature window, where optimal grip is achieved. The carcass temperature, on the other hand, reacts more slowly, making it more difficult to manage. This is particularly true in cases where carcass-temperature reductions are required. By integrating the temperature-sensitive wear rate, it is possible to track accumulated tyre wear and its subsequent impact on the car's performance. Tyre wear is modelled as a function of tread temperature and the friction power generated in the tyres' contact region. Each tyre compound has its own unique friction and wear characteristics and will respond differently to wear. The model presented can be used to help determine the point at which tyre wear compromises performance to such an extent that the tyres are no longer viable. Increases in track temperature are found to result in reduced tyre wear (for the tyre data used here). Similar sensitivity studies could be carried out in much the same way. It is hoped that this study can be used to gain competitive advantage and improve tyre management strategies.

REFERENCES

[1] H. J. Sussmann and J. C. Willems, "300 years of optimal control: from the brachystochrone to the maximum principle," *IEEE Control Systems Magazine*, vol. 17, no. 3, pp. 32–44, 1997.

[2] L. S. Pontryagin, *Mathematical Theory of Optimal Processes.* CRC Press, 2018.

[3] M. A. Patterson and A. V. Rao, "GPOPS-II: A MATLAB Software for Solving Multiple-Phase Optimal Control Problems Using hp-Adaptive Gaussian Quadrature Collocation Methods and Sparse Nonlinear Programming," *ACM Trans. Math. Softw.*, vol. 41, no. 1, pp. 1:1—-1:37, Oct 2014.

[4] J. P. M. Hendrikx, T. J. J. Meijlink, and R. F. C. Kriens, "Application of Optimal Control Theory to Inverse Simulation of Car Handling," *Vehicle System Dynamics*, vol. 26, no. 6, pp. 449–461, Dec 1996.

[5] V. Cossalter, M. Da Lio, R. Lot, and L. Fabbri, "A General Method for the Evaluation of Vehicle Manoeuvrability with Special Emphasis on Motorcycles," *Vehicle System Dynamics*, vol. 31, no. 2, pp. 113–135, Feb 1999.

[6] R. S. Sharp and H. Peng, "Vehicle dynamics applications of optimal control theory," *Vehicle System Dynamics*, vol. 49, no. 7, pp. 1073–1111, Jul 2011.

[7] G. Perantoni and D. J. N. Limebeer, "Optimal control for a Formula One car with variable parameters," *Vehicle System Dynamics*, vol. 52, no. 5, pp. 653–678, May 2014.

[8] D. J. N. Limebeer, G. Perantoni, and A. V. Rao, "Optimal control of Formula One car energy recovery systems," *International Journal of Control*, vol. 87, no. 10, pp. 2065–2080, Oct 2014.

[9] H. Pacejka, *Tire and Vehicle Dynamics*. Elsevier, 2005.

[10] G. Perantoni and D. J. N. Limebeer, "Optimal Control of a Formula One Car on a Three-Dimensional Track—Part 1: Track Modeling and Identification," *Journal of Dynamic Systems, Measurement, and Control*, vol. 137, no. 5, May 2015.

[11] D. J. N. Limebeer and G. Perantoni, "Optimal Control of a Formula One Car on a Three-Dimensional Track—Part 2: Optimal Control," *Journal of Dynamic Systems, Measurement, and Control*, vol. 137, no. 5, May 2015.

[12] M. I. Masouleh and D. J. N. Limebeer, "Heave spring and ride height optimisation of a Formula One car suspension system," in *2015 54th IEEE Conference on Decision and Control (CDC)*, 2015, pp. 165–170.

[13] M. Masouleh and D. Limebeer, "Optimizing the Aero-Suspension Interactions in a Formula One Car," *IEEE Transactions on Control Systems Technology*, vol. 24, no. 3, pp. 912–927, 2016.

[14] A. J. Tremlett and D. J. N. Limebeer, "Optimal tyre usage for a Formula One car," *Vehicle System Dynamics*, vol. 54, no. 10, pp. 1448–1473, Oct 2016.

[15] N. Dal Bianco, R. Lot, and M. Gadola, "Minimum time optimal control simulation of a GP2 race car," *Proceedings of the Institution of Mechanical Engineers, Part D: Journal of Automobile Engineering*, vol. 232, no. 9, pp. 1180–1195, Oct 2017.

[16] D. S. Naidu, *Optimal Control Systems*, ser. Electrical Engineering Series. CRC Press, 2002.

[17] B. A. Conway, "A Survey of Methods Available for the Numerical Optimization of Continuous Dynamic Systems," *Journal of Optimization Theory and Applications*, vol. 152, no. 2, pp. 271–306, 2012.

[18] A. V. Rao, "A survey of numerical methods for optimal control," *Advances in the Astronautical Sciences*, vol. 135, no. 1, pp. 497–528, 2009.

[19] J. T. Betts, *Practical Methods for Optimal Control and Estimation Using Nonlinear Programming*. Society for Industrial and Applied Mathematics, 2010.

[20] D. J. N. Limebeer and A. V. Rao, "Faster, Higher, and Greener: Vehicular Optimal Control," *IEEE Control Systems Magazine*, vol. 35, no. 2, pp. 36–56, 2015.

[21] A. Wächter and L. T. Biegler, "On the implementation of an interior-point filter line-search algorithm for large-scale nonlinear programming," *Mathematical Programming*, vol. 106, no. 1, pp. 25–57, 2006.

[22] P. E. Gill, W. Murray, and M. A. Saunders, "SNOPT: An SQP Algorithm for Large-Scale Constrained Optimization," *SIAM Review*, vol. 47, no. 1, pp. 99–131, Jan 2005.

[23] M. J. Weinstein and A. V. Rao, "Algorithm 984: ADiGator, a Toolbox for the Algorithmic Differentiation of Mathematical Functions in MATLAB Using Source Transformation via Operator Overloading," *ACM Trans. Math. Softw.*, vol. 44, no. 2, Aug 2017.

[24] A. Griewank and A. Walther, *Evaluating derivatives: principles and techniques of algorithmic differentiation*. Siam, 2008, vol. 105.

[25] A. Gent and J. Walter, *The Pneumatic Tire*. Mechanical Engineering Faculty Research, 2006.

[26] D. P. Kelly, "Lap Time Simulation with Transient Vehicle and Tyre Dynamics," Doctor of Philosophy, Cranfield University, May 2008.

[27] D. P. Kelly and R. S. Sharp, "Time-optimal control of the race car: influence of a thermodynamic tyre model," *Vehicle System Dynamics*, vol. 50, no. 4, pp. 641–662, Apr 2012.

[28] F. Farroni, M. Russo, A. Sakhnevych, and F. Timpone, "TRT EVO: Advances in real-time thermodynamic tire modeling for vehicle dynamics simulations," *Proceedings of the Institution of*

Mechanical Engineers, Part D: Journal of Automobile Engineering, vol. 233, no. 1, pp. 121–135, Nov 2018.

[29] A. Corollaro, "Essentiality of Temperature Management while Modeling and Analyzing Tires Contact Forces," Doctor of Philosophy, UNIVERSITA' DEGLI STUDI DI NAPOLI FEDERICO II, 2014.

[30] F. Farroni, D. Giordano, M. Russo, and F. Timpone, "TRT: thermo racing tyre a physical model to predict the tyre temperature distribution," *Meccanica*, vol. 49, no. 3, pp. 707–723, 2014.

[31] F. Farroni, "Development of a grip & thermodynamics sensitive tyre/road interaction forces characterization procedure employed in high-performance vehicles simulation," 2014.

[32] F. Farroni, A. Sakhnevych, and F. Timpone, "An evolved version of thermo racing tyre for real time applications," in *Proceedings of the World Congress on Engineering 2015 Vol II*, vol. 2218, London, 2015, pp. 1159–1164.

[33] F. Farroni, M. Russo, R. Russo, and F. Timpone, "A physical-analytical model for a real-time local grip estimation of tyre rubber in sliding contact with road asperities," *Proceedings of the Institution of Mechanical Engineers, Part D: Journal of Automobile Engineering*, vol. 228, no. 8, pp. 955–969, Feb 2014.

[34] F. Farroni, A. Sakhnevych, and F. Timpone, "Physical modelling of tire wear for the analysis of the influence of thermal and frictional effects on vehicle performance," *Proceedings of the Institution of Mechanical Engineers, Part L: Journal of Materials: Design and Applications*, vol. 231, no. 1-2, pp. 151–161, Feb 2017.

[35] A. G. Veirh, "A Review of Important Factors Affecting Treadwear," *Rubber Chemistry and Technology*, vol. 65, no. 3, pp. 601–659, Jul 1992.

[36] A. H. Muhr and A. D. Roberts, "Rubber abrasion and wear," *Wear*, vol. 158, no. 1, pp. 213–228, 1992.

[37] A. Schallamach and D. M. Turner, "The wear of slipping wheels," *Wear*, vol. 3, no. 1, pp. 1–25, 1960.

[38] M. Gipser, "FTire – the tire simulation model for all applications related to vehicle dynamics," *Vehicle System Dynamics*, vol. 45, no. sup1, pp. 139–151, Jan 2007.

[39] B. N. Persson, "Theory of rubber friction and contact mechanics," *Journal of Chemical Physics*, vol. 115, no. 8, pp. 3840–3861, Aug 2001.

[40] A. Schallamach, "Recent Advances in Knowledge of Rubber Friction and Tire Wear," *Rubber Chemistry and Technology*, vol. 41, no. 1, pp. 209–244, Mar 1968.

[41] B. N. J. Persson and E. Tosatti, "Qualitative theory of rubber friction and wear," *The Journal of Chemical Physics*, vol. 112, no. 4, pp. 2021–2029, Jan 2000.

[42] D. J. N. Limebeer and M. Massaro, *Dynamics and Optimal Control of Road Vehicles*, 1st ed. Oxford University Press, 2018.

[43] P. Haney, *The racing and high-performance tire : using the tires to tune for grip and balance*. Warrendale, P.A SE - 286 pages: Society of Automotive Engineers, 2003.

[44] J. E. Mark, B. Erman, and C. M. Roland, *The Science and Technology of Rubber Fourth Edition*. Boston: Academic Press, 2013.

[45] S. K. Clark and R. N. Dodge, "Heat generation in aircraft tires," *Computers & Structures*, vol. 20, no. 1, pp. 535–544, 1985.

[46] Y. A. Cengel and J. M. Cimbala, *Fluid mechanics : fundamentals and applications*. McGraw-Hill, 2014.

[47] Collantine Media Ltd., "2019 Italian GP interactive F1 lap charts, times and tyres | RaceFans," 2019. [Online]. Available: https://www.racefans.net/2019/09/08/2019-italian-grand-prix-interactive-data-lap-charts-times-and-tyres/

ADDENDUM A DATA VISUALISATION TOOL
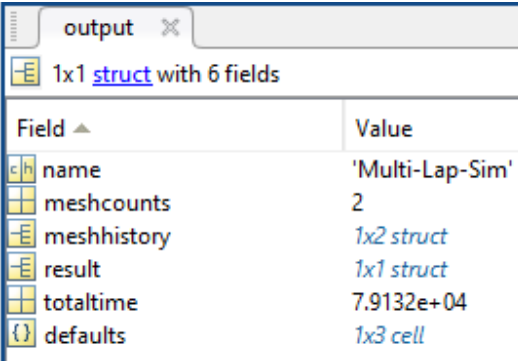
A.1 CHAPTER OVERVIEW

A data visualisation tool has been developed to interact with the result files that are produced by GPOPS-II. Matlab is used to convert the MAT-file into comma-separated values (CSV) files which are imported by a Microsoft Power BI report. The desktop application is free to download and has therefore been considered an appropriate platform to develop this tool. The report provides an elegant interface that can be used to view the model's state and control variables which will help racing teams to interpret the optimal control solution.

A.2 DATAFLOW

Once the optimal control problem has been solved by GPOPS-II, the results are saved in a MAT-file (a file produced in Matlab that has a .mat file extension). This file can be interpreted by Matlab and consists of various nested structured arrays. Figure A.1 shows an example of a GPOPS-II resultant MAT-file that is opened using the Matlab variable explorer. This file format is not easily accessible by third-party applications such as Power BI and has to be converted into a format that is easy to work with.

A Matlab program has been written that will extract the relevant data from the MAT-file and save it into multiple CSV files. This process consists of two parts: (i) extracting the state and control variables for each lap and (ii) calculating the track position in Cartesian coordinates. These CSV files form the building blocks for Power BI to further manipulate the data so that it can ultimately be trended in a user friendly interface.

Figure A.1. MAT-file produced by GPOPS-II

A.3   USER GUIDE

The report consists of multiple pages that focus on different aspects of the optimal solution. Each page is populated with either a single or multiple line charts that have certain interactions associated with it. A screenshot of each page is given in Figure A.2 to A.6. Annotations highlighting how the user can interaction with the tool are included in Figures A.2 and A.3, and are summarised as follows:

- The optimal control problem has been solved over multiple laps. By default the report plots a variable over the racing distance of 15 laps. The user can zoom in on a particular lap by selecting a lap number from the pane on the left side of the sceen. If a new lap is selected, it will override the previous selection unless the new lap is selected while holding down the Ctrl-key.

- The exact value of a data point can be viewed by hovering the cursor over the chart. A pop-up banner will appear together with a hairline to give additional information.

- Some of the pages have multiple charts which have been resized to fit on a single page. A full screen view of a particular chart can be obtained by clicking on the *Focus Mode* button in the top right corner of the chart.

- The *Track* page plots the track boundaries (Tlb & Trb) and racing line for each lap. By default the report shows the entire track. The buttons on the right side of the screen allows the user to zoom in on certain corners to view the racing line in more detail. A button is selected by holding the Ctrl-key while clicking on the button. The *Reset* button will restore the default view that shows the entire track.
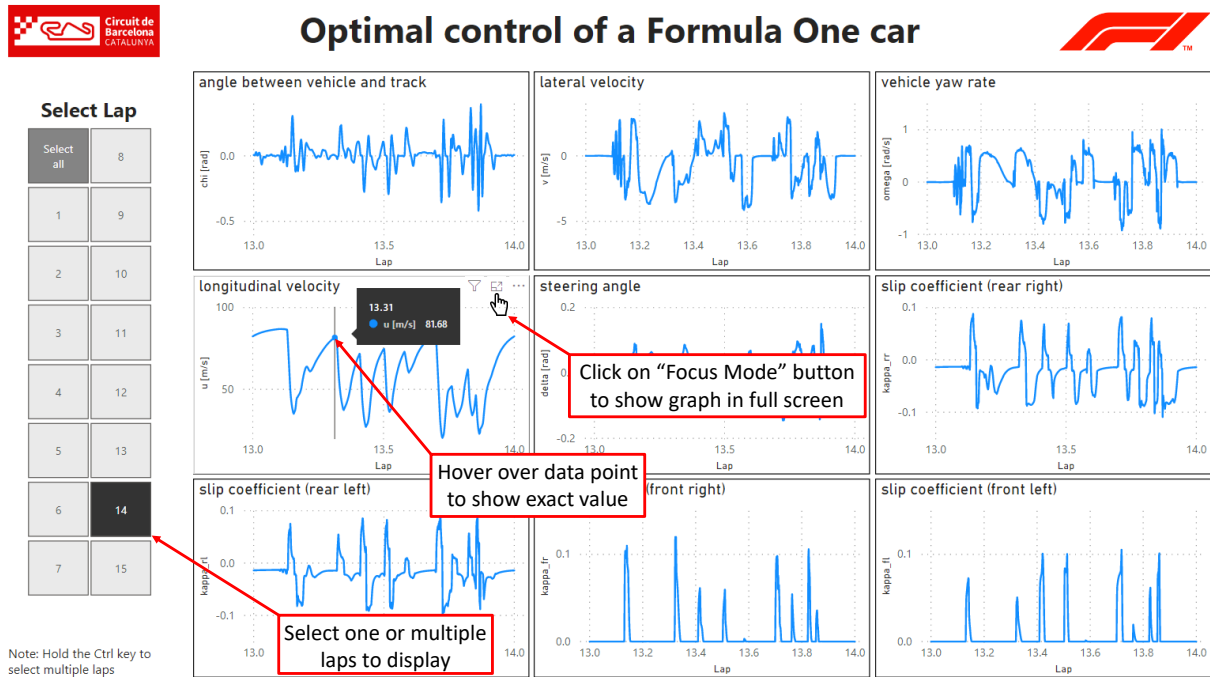
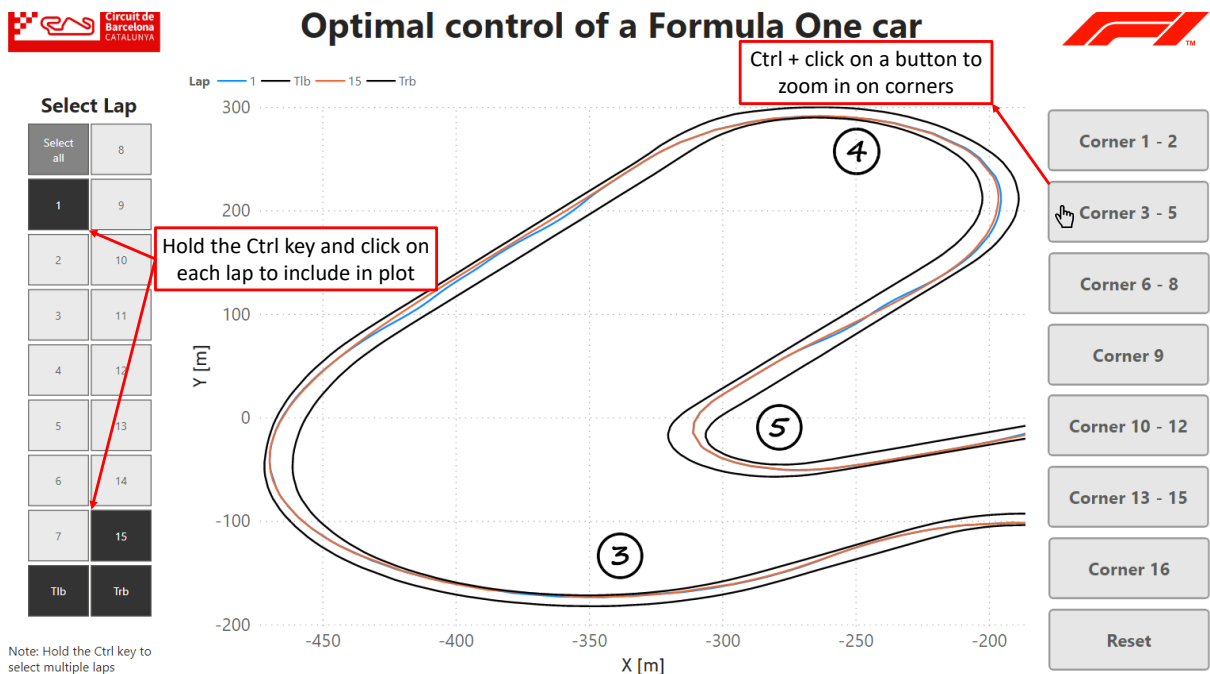**Figure A.2.** Screenshot of *States* page with annotations.

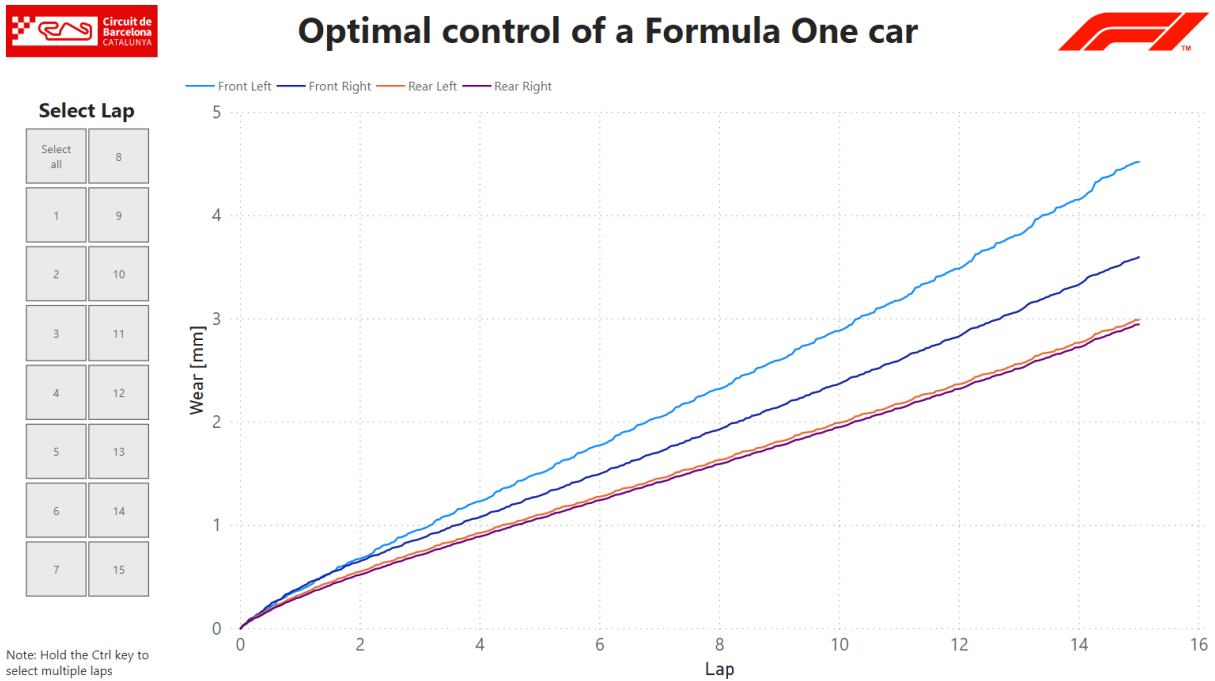**Figure A.3.** Screenshot of *Track* page with annotations.

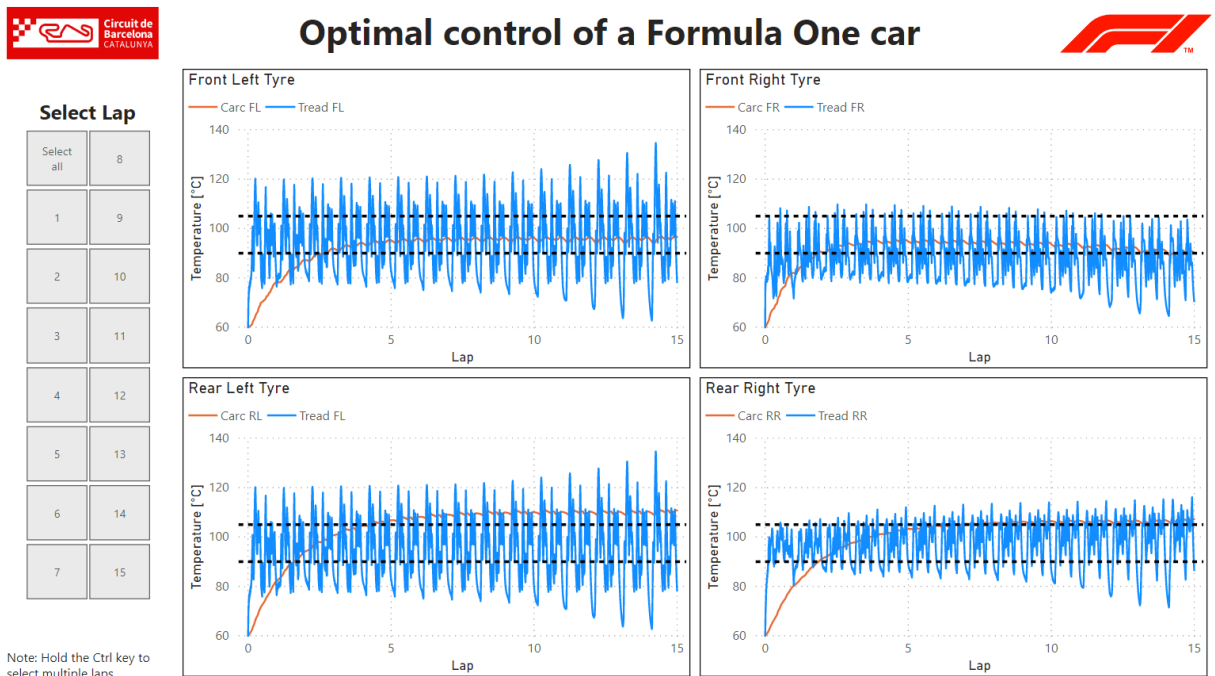**Figure A.4.** Screenshot of *Wear* page.

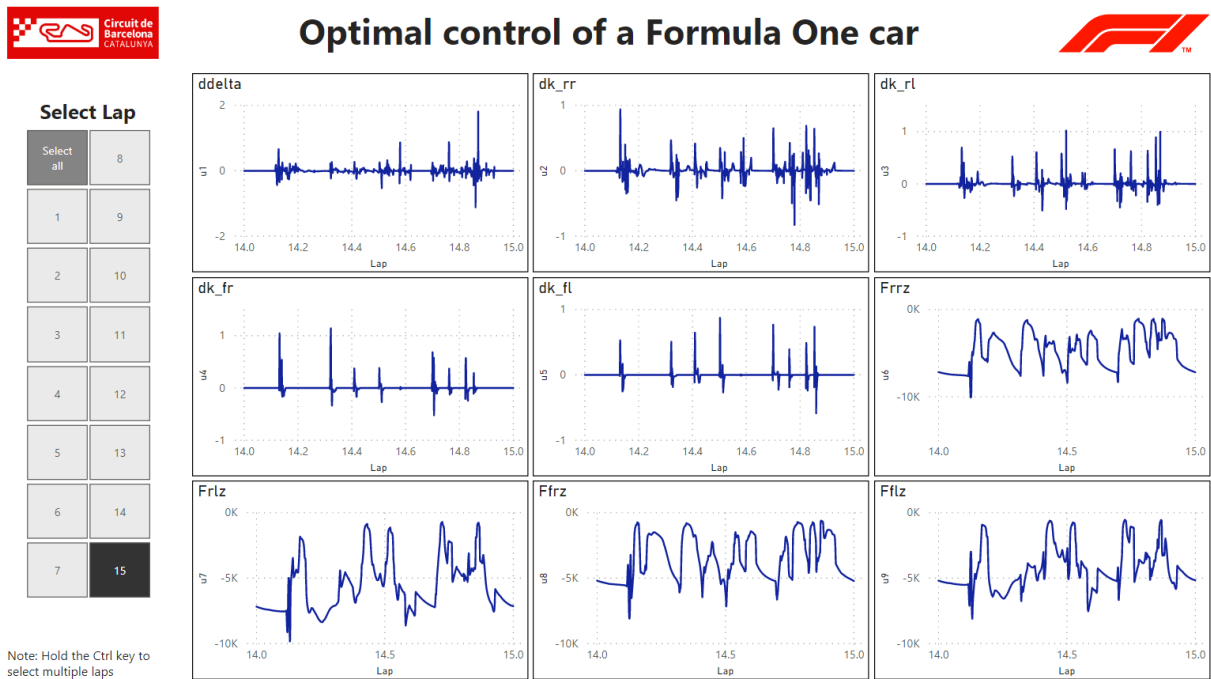
Figure A.5. Screenshot of *Tempearture* page.

Figure A.6. Screenshot of *Controls* page.

ADDENDUM B   MODEL PARAMETERS

Table B.1. Thermodynamic parameters [14]

Parameter	Description	Units	Value
T_{amb}	Track air temperature	°C	25
T_{track}	Track surface temperature	°C	35
m_t	Tyre tread mass	kg	0.5
m_c	Tyre carcass mass (front)	kg	9.5
	Tyre carcass mass (rear)	kg	11.5
c_t	Heat capacity of tread	kJ/kg K	2.4
c_c	Heat capacity of carcass	kJ/kg K	1.6
h_{tt}	Track-tyre heat transfer coefficient	kW/m^{2}K	12
c_{wf}	Contact patch width (front)	m	0.20
c_{wr}	Contact patch width (rear)	m	0.22
a_{cp}	Contact patch length constant	m/kN	0.056
α_c	Reference sliding/non-sliding slip angle	°	8
c_{s1}	Sliding/non-sliding reference 1	-	0.3
c_{s2}	Sliding/non-sliding reference 2	-	0.8
k_1	Strain parameter in the x-direction	m	0.1
k_2	Strain parameter in the y-direction	m	0.1
k_3	Strain parameter in the z-direction	m	1.0
D	Tyre diameter	m	0.66
W	Tyre width (front)	m	0.355
	Tyre width (rear)	m	0.380

Table B.2. Vehicle parameters [14]

Parameter	Description	Units	Value
P_{max}	Peak engine power	kW	560
M	Vehicle mass	kg	660
I_z	Moment of inertia about the z-axis	kg m^2	450
w	Wheelbase	m	3.4
a	Distance of the mass centre from the front axle	m	1.8
b	Distance of the mass centre from the rear axle	m	1.6
h	Centre of mass height	m	0.3
D_{roll}	Roll moment distribution (fraction at the front axle)	-	0.5
w_f	Front wheel to car centre line distance	m	0.73
w_r	Rear wheel to car centre line distance	m	0.73
R	Wheel radius	m	0.33
k_d	Differential friction coefficient	N/rpm	100

Table B.3. Tyre friction parameters [14]

Parameter	Description	Units	Value
F_{z1}	Reference load 1	N	2000
F_{z2}	Reference load 2	N	6000
$\mu_{x\max 1}$	Peak longitudinal friction coefficient at load 1	-	1.75
$\mu_{x\max 2}$	Peak longitudinal friction coefficient at load 2	-	1.40
$\mu_{y\max 1}$	Peak lateral friction coefficient at load 1	-	1.80
$\mu_{y\max 2}$	Peak lateral friction coefficient at load 2	-	1.45
$\kappa_{\max 1}$	Slip coefficient for the friction peak at load 1	-	0.11
$\kappa_{\max 2}$	Slip coefficient for the friction peak at load 2	-	0.10
$\alpha_{\max 1}$	Slip angle for the friction peak at load 1	°	9
$\alpha_{\max 2}$	Slip angle for the friction peak at load 2	°	8
Q_x	Longitudinal shape factor	-	1.9
Q_y	Lateral shape factor	-	1.9

Table B.4. Tyre wear parameters [14]

Parameter	Description	Units	Value
w_{p1}	Frictional power gain factor	mm/s	0.09
w_{p2}	Frictional power exponent	-	1.6
Q_{ref}	Reference frictional power	kW	150
w_{g1}	Graining gain factor	mm/°C s	0.4×10^{-5}
w_{g2}	Graining exponent	-	2
T_{tp}	Wear transition temperature	°C	100
w_{b1}	Blistering gain factor	mm/°C s	0.8×10^{-5}
w_{b2}	Blistering exponent	-	2

Table B.5. Fitted thermodynamic constants for each tyre

Parameter	Front left	Front Right	Rear left	Rear right
p_1	0.7291	0.5670	0.5071	0.6124
p_2	0.0060	0.0000	0.0125	0.0000
p_3	252.53	263.48	174.93	181.38